Observer–Based Control for a New Stochastic Maximum Power Point tracking for Photovoltaic Systems With Networked Control System

Muhammad Shamrooz Aslam, Prayag Tiwari ⓘ, Hari Mohan Pandey ⓘ Shahab S. Band

Abstract—This study discusses the new stochastic *maximum power point tracking (MPPT)* control approach towards the *photovoltaic cells (PCs)*. *PC* generator is isolated from the grid, resulting in a *direct current (DC)* microgrid that can provide changing loads. In the course of the nonlinear systems through the time-varying delays, we proposed a *Networked Control Systems (NCSs)* beneath an event-triggered approach basically in the fuzzy system. In this scenario, we look at how random, variable loads impact the *PC* generator's stability and efficiency. The basic premise of this article is to load changes and the value matching to a Markov chain. *PC* generators are complicated nonlinear systems that pose a modeling problem. Transforming this nonlinear *PC* generator model into the *Takagi–Sugeno (T–S) fuzzy* model is another option. *Takagi–Sugeno (T–S) fuzzy* model is presented in a unified framework, for which 1) the fuzzy observer–based on this premise variables can be used for approximately in the infinite states to the present system, 2) the fuzzy observer–based controller can be created using this same premises be the observer, and 3) to reduce the impact of transmission burden, an event-triggered method can be investigated. Simulating in the *PC* generator model for the real-time climate data obtained in China demonstrates the importance of our method. In addition, by using a new *Lyapunov–Krasovskii functional (LKF)* for combining to the allowed weighting matrices incorporating mode-dependent integral terms, the developed model can be stochastically stable and achieves the required performances. Based on the *T-P transformation*, a new depiction of the nonlinear system is derived in two separate steps in which an adequate controller input is guaranteed in the first step and an adequate vertex polytope is ensured in the second step.

To present the potential of our proposed method, we simulate it for *PC* generators.

Index Terms—Observer–based control; Photovoltaic cell arrays; maximum power point tracking; Linear matrix inequalities (LMIs).

I. INTRODUCTION

GLOBAL energy consumption is increasing as a result of rising living standards, a growing global population, and considerable increases in national income [1]. However,

M.S. Aslam is with the School of Automation, Guangxi University of Science and Technology, Liuzhou, P.O. Box 545006 P.R. China. Email: shamroz_aslam@yahoo.com

P. Tiwari is with the Department of Computer Science, Aalto University, Espoo, Finland; Email: prayag.tiwari@aalto.fi

H.M. Pandey is with Data Science and Artificial Intelligence, Department of Information and Computing, Bournemouth University, UK; Email: profharimohanpandey@gmail.com

Shahab S. Band is with the Future Technology Research Center, College of Future, National Yunlin University of Science and Technology, Douliou, Taiwan, ROC; Email: shamshirbands@yuntech.edu.tw

Corresponding Authors: Hari Mohan Pandey, Prayag Tiwari, S. Shamshirband

to fulfil global energy demand massive dependency on traditional fuels (gas, coal, and oil) causes environmental issues including carbon emissions, climate change, and unpredictable weather [2]. While on the other side, a growing global energy demand has made confirming the production of electricity an increasingly important issue. It is widely recognized that photovoltaic power is a renewable energy source due to its reputation as being a reliable, sustainable and often low-maintenance energy source. It would not only have an impact on human health, but it also has an impact on economic development. Therefore, the need for a renewable and sustainable energy source has prompted the power sector throughout the world to investigate the feasibility of bulk power generation applying renewable energy sources (wind energy, photovoltaic energy, and hydro-electric energy) [3], nonlinear control design [4], [5]. In this perspective, photovoltaic energy is considered as one of the finest options for dealing with climate change, since it is a reliable and sustainable energy source that requires minimal maintenance work; for additional details, please see references [6], [7]. Solar–based generation, in which sunlight is directly transformed into electricity, has gained popularity in recent decades due to an exponential drop in energy generation costs. Currently, *PCs* with output power oscillating in the milli-watts for scientific calculators are being produced and installed in residential/industrial solar farms [8]. It is worth mentioning that *PC generators* have not only impact on the theoretical aspects but also have strong influence on the practical and engineering applications. In this aspect, increasing the efficiency of the *PC system* is critical for optimal functioning. When it comes to the technical elements of solar systems with various loads, it can be well recognized that energy required by these loads may fluctuate erratically and unpredictably [9]. The reason for this is the nonlinear characteristic of photovoltaic system output, and its dependency on temperature change and ambient light. To cope with load fluctuation, we may use stochastic systems to model such load variations. It can also characterize solar systems under three distinct situations: (1) variable load demand, (2) random variations of environmental conditions, (3) and varying supply profile [10]. The stochastic characterization of the changing load is critical for guaranteeing the stability and efficiency of the *PC system*. In this instance, a study [12] describes a method for accounting for stochastic uncertainty. In this regard, it is important to study the *PC* in which authors explore the properties of power generators.

To make best use of photovoltaic arrays, the system must attain a *maximum power point (MPP)* equilibrium [11]. The procedure for locating this *MPP* in the nonlinear region of *I–V curve* is identified as, *maximum power point tracking (MPPT)*. Thus, to enhance complete system efficiency, *MPPT* is required in the operation of *PC arrays* [12]. This technique can constantly adjust load (duty cycle) while maximizing panel power output. In this scientific literature, several *MPPT* control techniques have been proposed. According to the literature, *MPPT algorithms* can be classified into two parts: classic and modern. The most common used classic *MPPT* approaches are *perturb–and-observe (PO)*, the *incremental conductance (IC)*, *fractional open circuit voltage (FCV)*, *fractional short-circuit current (FCC)*, and *hill climbing (HC)* [13]–[17]. On other side *artificial neural networks (ANN)* [18] and *fuzzy logic control (FLC)* [19]; were considered as an modern *MPPT approaches*, for further information, see [20] and references therein. The results of *ANN* are promising, however, they need a significant volume of data which must include information about the characteristics of the *PC cell*, such as insolation, and temperature. The fuzzy logic, on the other hand, is adaptable because it does not require massive data sets. Due to the unique properties of T-S, fuzzy systems, we incorporate the features of T-S fuzzy systems with *PC generators*. As a result, this article supports the T–S fuzzy method.

In practical applications, uncertainties and disturbances constantly have an impact on nonlinear systems [21], [22]. Both uncertainties and system disturbances can make controller design extremely difficult, and may even cause the system's performance to degrade. It is necessary to investigate and explore new techniques to overcome such kinds of difficulties. It will be more meaningful to implement the new design method for the power systems specially for photovoltaic cells. The *PC system* is no exception; disturbance and uncertainty have a significant impact on it, which causes frequency deviation. These are the basis for the feedback control approach for frequency deviation control of *PC systems*. The feed–forward controller works differently, changing the system's input based on the disturbance signal or its estimation. In essence, the controller takes the appropriate action by properly setting the system input prior to having the consequences of disturbances on the system outputs. To encounter the tracking problem with system disturbances, *observer-based control (OBC)* has a huge significance for nonlinear systems. In this regard, several authors investigate the properties of *OBC*, e.g., Mechanical plants [23], [24], Aircraft systems [25], [26], and nonlinear system [27]. In [25], the author investigated the disturbance observer-based control mechanism for the *UAV* system in the form of transient observation, while [27] researchers focused on the phenomenological bioreactor model to the proposed methodology for the efficient production of the chemical reactor. In [28] and [29], authors developed the new observer-design model for a networked system under time-varying delays. Based upon the above discussion and
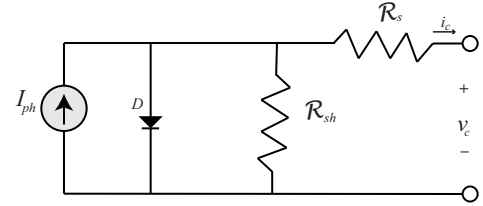

Fig. 1: Circuit diagram of solar panel.

according to the author's knowledge, there was no work on the observer-based controller for the *PC systems* with the consideration *MPPT*.

In this paper, we discuss a well-adjusted representation in a relaxed feedback control environment that provides a good representation of a nonlinear system. A well-adjusted representation is calculated using the *T–P model* transformation. An *LPV system* can be transformed into a *T–P model* using this transformation, first introduced by *Baranyi* [38]. After normalizing the conversion functions towards convex combinations, which is a main step in the transformation of *T–P models*, the resultant *T–P model* remains polytopic. The authors of this paper propose a less accurate polytopic representation of the nonlinear system in order to relax the conservatism of the nonlinear control solution characterized by *LMIs*. A well-relaxed nonlinear controller can be achieved by implementing the *T–P model* algorithm.

The difficulties and challenges of this research come from the original scenario that observer-based control (especially stability analysis) of closed-loop error systems has been investigated under the unified structure of event-driven scheme for photovoltaic model. For a limited time limit, the *Zeno behavior* must be excluded to eschew unlimited driving samplings. Furthermore, we consider the *Markov-driven load* in this paper in order to consider *MPPT*. Among the novel aspects of this work is the setup. Several of these works concern approximation and produce results that are less conservative than those presented in these studies.

- The primary contribution of this article is the combination of an observer-based T–S fuzzy method with *PC* array stochastic control. This configuration makes the *PC* arrays more resistant to the unpredictability of weather and load changes. Under random load variations, the underlying *MPPT* control mechanism stays stable, the load varies according to a continuous–time Markov chain.
- Secondly, our approach's efficiency is demonstrated by a simulation based on real–time data obtained in China. When the load changed rapidly, the oscillations around the *MPP* were suppressed. The findings imply that the *PC* generator is stable, even when the load varies randomly, which is consistent with the theoretical result presented in this work.
- On the basis of *LMIs*, a novel Lyapunov functional can be proposed to establish acceptable circumstances and stochastically stabilize the system, resulting in delay–dependent conditions. Along with the event–triggered

system, our suggested methodology enables excellent bandwidth usage. The *PC* generator verifies it.

Notations: Most of the symbols are generalized and standard, and well represented in the existing literature. Particularly, $'I'$ presents for an identity matrix of proper dimension; Diagonal matrix denotes by $diag(...)$; The induced symmetry terms presented by $'\heartsuit'$; Transpose of the matrix denotes by "T".

II. MATHEMATICAL MODELING OF PHOTOCELL ARRAY WITH LOAD USING THE MARKOV PROCESS PHENOMENA

The *PC* model which will be represented in the circuit shown in Fig. 1 for converting sunlight into energy [31], [32]. The current source $\mathcal{I}_{ph}$ is linked in parallel to a diode D, and these resistances $\mathcal{R}_s$ and $\mathcal{R}_{sh}$ obey a relationship for the value of $\mathcal{R}_s$ can be ignored when compared to that the value of $\mathcal{R}_{sh}$ [33]. This feature is taken into account in the model that follows.

A *PC* cell's output voltage-current characteristic is expressed as follows [34]:

$$i_c = \mathcal{I}_{ph} - \mathcal{I}_{rs} \exp^{\aleph_1} \tag{1}$$

where

$$\aleph_1 = \left(\frac{q v_c}{\eta k \mathcal{T}} \right) - 1$$

In above, i_c and v_c are the current for the solar cell and the output voltage; q denoted in electronic charge, which can be $1.6 \times 10^{-19} C$; η is an diode's ideality factor; in this *Boltzman constant* (k) is $1.3805 \times 10^{-23} J/K$. The *PC* is installed in n_p parallel strings; which is made up to an n_s connecting cells in this series, producing enough power to power the linked load. The electrical characteristic of the *PC* is expressed by the equation below:

$$i_{pc} = n_p \left(\mathcal{I}_{ph} - \mathcal{I}_{rs} \exp^{\aleph_2} \right) \tag{2}$$

where

$$\aleph_2 = \frac{q v_{pc}}{\eta k \mathcal{T}} - 1$$

The *PC* output current and voltage shall be represented by i_{pc} and v_{pc}, respectively. $\mathcal{I}_{ph}$ (light-produced current) and $\mathcal{I}_{rs}$ (reverse saturation current) are two currents that are generated by light. According to the following equations, $\mathcal{I}_{rs}$ is dependent on cell temperature $\mathcal{T}$ and insolation λ [31], [32].

$$\begin{cases} \mathcal{I}_{ph} &= (\mathcal{I}_{sc} + \mathcal{K}_I(\mathcal{T} - \mathcal{T}_r)) \frac{\lambda}{\lambda_\mathcal{T}} \\ \mathcal{I}_{rs} &= \mathcal{I}_{rr} \left(\frac{\mathcal{T}}{\mathcal{T}_r} \right)^3 exp \left(\frac{q\mathcal{E}_{gp}}{\eta k} \left(\frac{1}{\mathcal{T}} - \frac{1}{T_T} \right) \right) \end{cases} \tag{3}$$

The short–circuit cell power at orientation temperature and insolation was $\mathcal{I}_{sc}$, in this temperature coefficient of short–circuit current is $\mathcal{K}_I$, in an opposite saturation current at an orientation temperature is $\mathcal{I}_{rr}$, remain the band-gap energy to the cell's semiconductor is $\mathcal{E}_{gp} = 1.1eV$.

In the *PC* generator system is formed by connecting the *PC*, also known as a *PC* panel, to other components (see Fig. 2). The *PC* generating system, as can be seen, contains a DC–DC converter circuit, as well as a inductor, capacitor, a diode, resistances, and a *MOSFET*, which are all connected to the *PC module*. This circuit operates by having a signal at $u(t)$
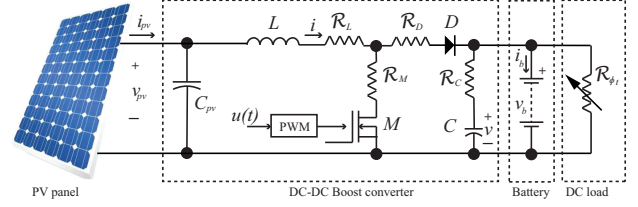

Fig. 2: Circuit diagram of solar panel.

direct a *MOSFET* to yield current through the circuit in the sequence indicated.

III. SWITCHING LOAD USING THE STOCHASTIC PROCESS

The *PC* arrays in this article are meant to supply an set of various *DC* loads that can randomly activate and deactivate to varying power profiles at any time. Because of this characteristic, global load demand is uncertain [35]. Markov chain, in particular, may be used to represent the unpredictable, sudden changes that occur in real-time operations [36]. Following that, we shall go over some basic Markov chain principles.

We suppose $\mathcal{S} := \{1, \cdots, s\}$ be an set indicating the load's operating modes. A continuous–time stochastic process $\{\phi_t, t \geq 0\}$ governs the modes, for the following transition probability:

$$Pr[\phi_{t+h} = m | \phi_t = n] = \begin{cases} \pi_{nm} h + o(h), & if \quad n \neq m, \\ 1 + \pi_{nn} h + o(h), & if \quad n = m, \end{cases} \tag{4}$$

where

$$\pi_{nn} = - \sum_{m:m \neq n} \pi_{nm}, \quad \pi \geq 0, n \neq m;$$

is this switch rate since the state n by instant t to state m to all $n, m \in \mathcal{S}$, however

$$\lim_{h \to 0} = \frac{o(h)}{h} = 0$$

In the sake of simplicity, we shall suppose which the *DC* load is *ON* by the time t, which corresponds for the resistive load focused in this stochastic process $\{\phi_t\}$. The variable resistor in the circuit is driven by $\{\phi_t\}$ and is represented simply by $\{\mathcal{R}_{\phi_t}\}$. The following relationship describes how load fluctuations impact the *PC* panel's output power [39]:

$$\mathcal{P}_{pc} = \mathcal{R}_{\phi_t} i_{pc}^2 (1 - u(t))^2 \tag{5}$$

The stochastic control approach depending on the dynamics of the *PC* generator will be presented in the sections that follow. The control goal assures the *PC* generator's stability as well as these maximum power point's chasing even when the load changes abruptly.

A. System Description

In the current section, we will show the dynamics of the system. Let us suppose $p(t) = \begin{bmatrix} v_{pc}(t) \\ i(t) \\ v(t) \end{bmatrix} \in \mathbf{R}^3$ represents the *PC* generator's system state, where $v_{pc}(t)$ presents the

TABLE I: **Nomenclature**

$\mathcal{P}_{max}$	Maximum power $[W]$	v_c	Output PC voltage $[V]$
i_c	Output PC current $[A]$	v_{pc}	PC voltage module output $[V]$
i_{pc}	PC current module output $[A]$	$\mathcal{V}_{mp}$	Maximum power voltage $[V]$
Voltages and Current:			
$\mathcal{I}_{mp}$	Maximum power current $[A]$	$\mathcal{V}_{oc}$	Voltage in an open circuit $[V]$
$\mathcal{I}_{ph}$	Current produced by light $[A]$	$\mathcal{I}_{rs}$	Saturation current in reverse $[A]$
$\mathcal{I}_{sc}$	Current in a short circuit $[A]$	$\mathcal{T}$	Temperature of the Cells $[°C]$
$\mathcal{T}_r$	Temperature of the reference cell $[°C]$	$\mathcal{G}$	Insolation $[W/m^2]$
$\mathcal{G}_r$	Reference insolation $[W/m^2]$	$\mathcal{K}_I$	Coefficient of temperature $[A/°C]$
Constant factors:			
k	Boltzman constant $[J/K]$	$\mathcal{E}_{gp}$	Energy in the band-gap $[eV]$
q	Charge of electrons $[C]$	$\mathcal{N}_s, \mathcal{N}_p$	Cells in a series-parallel configuration
η	Factor of ideality	ϕ_t	Markov process in continuous time
$\mathcal{C}_{pc}$	Capacitor at the input $[F]$	$\mathcal{C}$	Capacitor for the output $[F]$
Resistances:			
$\mathcal{R}_C$	Capacitor output resistance $[\Omega]$	$\mathcal{L}$	Inductance $[H]$
$\mathcal{R}_L$	Resistance to inductance $[\Omega]$	$\mathcal{R}_M$	MOSFET internal resistance $[\Omega]$
$\mathcal{R}_D$	Diode internal resistance $[\Omega]$	$\mathcal{R}_{\phi_t}$	Equivalent DC load activates at instant t $[\Omega]$
v_b	Battery voltage $[V]$	i_b	Battery current $[A]$

TABLE II: **Abbreviations**

T-S	Takagi-Sugeno
SCC	Short-circuit current
PC	Photovoltaic cell
LMIs	Linear matrix inequalities
MPPT	Maximum power point tracking
OCV	Open-circuit voltage
P & O	Perturb and observe
INC	Incremental conductance
DC	Direct-current
ANN	Artificial neural network

output voltage; $i(t)$ means the inductor current; and $v(t)$ denotes the capacitor voltage. The *MOSFET* duty cycle is controlled by the control input $u(t) \in \begin{bmatrix} 0 & 1 \end{bmatrix}$. As stated in [40], we depict the dynamics of the *PC* arrays by analyzing the *MOSFET*, while it is operating in either the "on" or "off" mode. The dynamics changes are present as:

$$\dot{p}(t) = \begin{cases} \mathcal{A}^{ON}\left(p(t),\phi_t\right)p(t) + \mathcal{B}^{ON}(\phi_t)p_b(t), \\ \quad When\ MOSFET\ turn\ ON \\ \mathcal{A}^{OFF}\left(p(t),\phi_t\right)p(t) + \mathcal{B}^{OFF}(\phi_t)p_b(t), \\ \quad When\ MOSFET\ turn\ OFF \end{cases}$$

where

$$\mathcal{A}^{ON} = \begin{bmatrix} \frac{1}{\mathcal{C}_{pc}}\frac{i_{pc}}{v_{pc}} & -\frac{1}{\mathcal{C}_{pc}} & 0 \\ \frac{1}{\mathcal{L}} & -\frac{\mathcal{R}_{\mathcal{L}}+\mathcal{R}_M}{\mathcal{L}} & 0 \\ 0 & 0 & -\frac{1}{\mathcal{C}(\mathcal{R}_C+\mathcal{R}_{\phi_t})}) \end{bmatrix}$$

$$\mathcal{B}^{ON} = \begin{bmatrix} 0 \\ 0 \\ -\frac{1}{\mathcal{C}(\mathcal{R}_C+\mathcal{R}_{\phi_t})} \end{bmatrix}$$

$$\mathcal{A}^{OFF} = \begin{bmatrix} \frac{1}{\mathcal{C}_{pc}}\frac{i_{pc}}{v_{pc}} & -\frac{1}{\mathcal{C}_{pc}} & 0 \\ \frac{1}{\mathcal{L}} & -\frac{\mathcal{R}_L+\mathcal{R}_D+\frac{\mathcal{R}_C\mathcal{R}_{\phi_t}}{\mathcal{R}_C+\mathcal{R}_{\phi_t}}}{\mathcal{L}} & -\frac{R_{\phi_t}}{\mathcal{L}(\mathcal{R}_C+\mathcal{R}_{\phi_t})} \\ 0 & \frac{\mathcal{R}_{\phi_t}}{\mathcal{C}(\mathcal{R}_C+\mathcal{R}_{\phi_t})} & -\frac{1}{\mathcal{C}(\mathcal{R}_C+\mathcal{R}_{\phi_t})}) \end{bmatrix}$$

$$\mathcal{B}^{OFF} = \begin{bmatrix} 0 \\ \frac{\mathcal{R}_{\phi_t}}{\mathcal{L}(\mathcal{R}_C+\mathcal{R}_{\phi_t})} \\ -\frac{1}{\mathcal{C}(\mathcal{R}_C+\mathcal{R}_{\phi_t})}) \end{bmatrix}$$

We get the following results using the time-averaging method, as mentioned in [40].

$$\begin{aligned} \dot{p}(t) = & \left\{ \mathcal{A}^{ON}\left(p(t),\phi_t\right)p(t) + \mathcal{B}^{ON}(\phi_t)p_b(t) \right\} u(t) \\ & + \left\{ \mathcal{A}^{OFF}\left(p(t),\phi_t\right)p(t) + \mathcal{B}^{OFF}(\phi_t)p_b(t) \right\} \\ & (1-u(t)) \end{aligned}$$

The *PC* array's power output is determined by

$$\begin{aligned} \mathcal{P}_{pc} &= i_{pc}v_{pc} \\ &= n_p\mathcal{I}_{ph}\mathcal{V}_{pc} - n_p\mathcal{I}_{rs}v_{pc}\left(\exp\left(\frac{k_{pc}v_{pc}}{n_s}\right) - 1\right) \end{aligned} \quad (6)$$

where, the inverse of the thermal voltage is denoted by

$$k_{pc} = \frac{q}{\eta k \mathcal{T}}$$

The *PC* power slope equals when the derivative of $\mathcal{P}_{pc}$ with respect to v_{pc} is calculated.

$$\begin{aligned} y(t) &= \frac{d\mathcal{P}_{pc}}{dv_{pc}} \\ &= i_{pc} - \frac{n_p k_{pc}}{n_s}\mathcal{I}_{rs}v_{pc}\exp\left(\frac{k_{pc}v_{pc}}{n_s}\right) \end{aligned} \quad (7)$$

In the series, $y(t)$ is an system output which should be pushed into zero in order for the *PC* array to operate at maximum power. In order to process this, we may join (6) and (7) to arrive at the conclusion that the *PC* generating system's nonlinear dynamics are as follows:

$$\begin{aligned} \dot{p}(t) &= \mathcal{A}(p(t),\phi_t)p(t) + \mathcal{B}(p(t),\phi_t)u(t) + \mathcal{E}_o(\phi_t)p_b(t) \\ x(0) &= x_0 \in \mathbf{R}^n, \quad \phi_0 \in \mathcal{S} \\ y(t) &= \mathcal{C}(p(t))p(t) \end{aligned}$$

where the matrices of the system are

$$\mathcal{A}(p(t),\phi_t) = \begin{bmatrix} \frac{1}{\mathcal{C}_{pc}}\frac{i_{pc}}{v_{pc}} & -\frac{1}{\mathcal{C}_{pc}} \\ \frac{1}{\mathcal{L}} & -\frac{\mathcal{R}_L+\mathcal{R}_D+\frac{\mathcal{R}_C\mathcal{R}_{\phi_t}}{\mathcal{R}_C+\mathcal{R}_{\phi_t}}}{\mathcal{L}} \\ 0 & \frac{\mathcal{R}_{\phi_t}}{\mathcal{C}(\mathcal{R}_C+\mathcal{R}_{\phi_t})} \end{bmatrix}$$

$$\mathcal{B}(p(t),\phi_t) = \begin{bmatrix} 0 \\ -\frac{\mathcal{R}_{\phi_t}}{\mathcal{L}(\mathcal{R}_C+\mathcal{R}_{\phi_t})} \\ -\frac{1}{\mathcal{C}(\mathcal{R}_C+\mathcal{R}_{\phi_t})}) \end{bmatrix}$$

$$\mathcal{B}(p(t),\phi_t) = \begin{bmatrix} 0 \\ -\frac{\mathcal{R}_{\phi_t}}{\mathcal{C}(\mathcal{R}_C+\mathcal{R}_{\phi_t})}i(t) \end{bmatrix}$$

$$\mathcal{E}_o(\phi_t) = \begin{bmatrix} 0 \\ \mathcal{B}_a \\ \frac{\mathcal{R}_C\mathcal{R}_{\phi_t}}{\mathcal{L}(\mathcal{R}_C+\mathcal{R}_{\phi_t})} \\ -\frac{\mathcal{R}_{\phi_t}}{\mathcal{C}(\mathcal{R}_C+\mathcal{R}_{\phi_t})}) \end{bmatrix}$$

$$\mathcal{C}(p(t)) = \begin{bmatrix} \frac{i_{pc}}{v_{pc}} - \frac{n_p k_{pc}}{n_s}\mathcal{I}_{rs}v_{pc}\exp\left(\frac{k_{pc}v_{pc}}{n_s}\right) & 0 & 0 \end{bmatrix}$$

where $\mathcal{B}_a = \frac{-\mathcal{R}_M+\mathcal{R}_D+\frac{\mathcal{R}_C\mathcal{R}_{\phi_t}}{\mathcal{R}_C+\mathcal{R}_{\phi_t}}}{\mathcal{L}}i(t) + \frac{\mathcal{R}_{\phi_t}}{\mathcal{L}(\mathcal{R}_C+\mathcal{R}_{\phi_t})}v(t) - \frac{\mathcal{R}_C\mathcal{R}_{\phi_t}}{\mathcal{L}(\mathcal{R}_C+\mathcal{R}_{\phi_t})}i_b(t)$.

It is tough to deal with the nonlinear, stochastic system (8). We reformulated the system (8) in the T–S fuzzy method in an attempt to overcome such a challenge.

B. Takagi Sugeno (T–S) System modeling

The T–S fuzzy method will be helpful for modeling nonlinear systems by combining local linear subsystems that are weighted by a membership function and rely on "IF–THEN" rules [41]. The *PV system* (8) is then converted into a T–S fuzzy form. The components of the premise–variable vectors are defined as below:

$$g(t) = \begin{bmatrix} g_1(t) \\ g_2(t) \\ g_3(t) \\ g_4(t) \\ g_5(t) \end{bmatrix} = \begin{bmatrix} \frac{i_{pc}(t)}{v_{pc}(t)} \\ i(t) \\ v(t) \\ i_b \\ \frac{n_p k_{pc}}{n_s}\mathcal{I}_{rs}v_{pc}\exp\left(\frac{k_{pc}v_{pc}(t)}{n_s}\right) \end{bmatrix}$$

Assume the next fuzzy rules:
Rule i: IF $g_1(t)$ **is** W_i^1 **and** $\cdots g_\varrho(t)$ **is** W_i^ϱ **THEN**

$$A_i(\phi_t) = \begin{bmatrix} \frac{1}{\mathcal{C}_{pc}}g_{i,1} & -\frac{1}{\mathcal{C}_{pc}} \\ \frac{1}{\mathcal{L}} & -\frac{\mathcal{R}_L+\mathcal{R}_D+\frac{\mathcal{R}_C\mathcal{R}_{\phi_t}}{\mathcal{R}_C+\mathcal{R}_{\phi_t}}}{\mathcal{L}} \\ 0 & \frac{\mathcal{R}_{\phi_t}}{\mathcal{C}(\mathcal{R}_C+\mathcal{R}_{\phi_t})} \end{bmatrix}$$

$$B_i(\phi_t) = \begin{bmatrix} 0 \\ -\frac{\mathcal{R}_{\phi_t}}{\mathcal{L}(\mathcal{R}_C+\mathcal{R}_{\phi_t})} \\ -\frac{1}{\mathcal{C}(\mathcal{R}_C+\mathcal{R}_{\phi_t})}) \end{bmatrix}$$

$$B_i(\phi_t) = \begin{bmatrix} 0 \\ \mathcal{B}_a^1 \\ -\frac{\mathcal{R}_{\phi_t}}{\mathcal{C}(\mathcal{R}_C+\mathcal{R}_{\phi_t})}g_i^2 \end{bmatrix}$$

$$C_i = \begin{bmatrix} g_i^1 - g_i^5 & 0 & 0 \end{bmatrix}$$

where $\mathcal{B}_a^1 = \frac{-\mathcal{R}_M+\mathcal{R}_D+\frac{\mathcal{R}_C\mathcal{R}_{\phi_t}}{\mathcal{R}_C+\mathcal{R}_{\phi_t}}}{\mathcal{L}}g_i^2 + \frac{\mathcal{R}_{\phi_t}}{\mathcal{L}(\mathcal{R}_C+\mathcal{R}_{\phi_t})}g_i^3 - \frac{\mathcal{R}_C\mathcal{R}_{\phi_t}}{\mathcal{L}(\mathcal{R}_C+\mathcal{R}_{\phi_t})}g_i^4$. The following is the membership function associated with the ith subsystem:

$$\hbar_i(g(t)) = \frac{W_i(g(t))}{\sum_{i=1}^s W_i(g(t))}, \qquad W_i(g(t)) = \prod_{j=1}^\varrho M_{i,j}(g_j(t))$$

For every $i \in \mathcal{M} := \{1,\cdots,r\}$, the following restrictions apply

$$\sum_{i=1}^s \hbar_i(g(t)) = 1, \quad 0 \le \hbar_i(g(t)) \le 1, \quad \forall t \ge 0 \qquad (8)$$

Where s denotes number of fuzzy rules and $W_j^i(g_j(t))$ is the membership activation degree of $g_j(t) \in [g_j^l \quad g_j^u]$ in fuzzy set $W_{i,j}$, given in the generic format.

$$W_j^l = \frac{g_j^u-g_j(t)}{g_j^u-g_j^l}, \qquad W_j^u = \frac{g_j(t)-g_j^l}{g_j^u-g_j^l} \qquad (9)$$

Finally, the *PC* generator's T–S fuzzy model is shown below:

$$\begin{aligned} \dot{p}(t) &= \sum_{i=1}^s \hbar_i(g(t))[\mathcal{A}_i(\phi_t)p(t) + \mathcal{B}_i(\phi_t)u(t) \\ &+ \mathcal{E}_o(\phi_t)p_b(t) \\ p(0) &= p_0 \in \mathbf{R}^n, \quad \phi_0 \in \mathbb{S} \\ y(t) &= \sum_{i=1}^s \hbar_i(g(t))\mathcal{C}_i p(t) \end{aligned} \qquad (10)$$

where the matrices $\mathcal{A}_i, \mathcal{B}_i$, and $\mathcal{C}_i$ for $\{i \in 1,\cdots,r\}$ are derived using the various combinations of the premise-variables.

C. Event-triggered control (ETC) scheme

A communication environment is used to control over a conventional *NCS*. To reduce the impact of communication load, an *ETC technique* is used. Due to network-induced interruption in sensor-to-controller interface, and this current premise variables in the fuzzy rule for systems and on the controller side will not be synchronous in *NCSs*. *ETC-approach* can be possible for computing the event generator through instant $i_k\mathbf{h}$ in this article. Peng and Yang [42] provide a logic function that compares the most recent sampled-data sent in that error among the present sampled-data and most recent sampled-data delivered. Our transmission method may decide whether the sampled data should be delivered or not:

$$e_k(t) = y(z_k\mathbf{h}) - y(i_k\mathbf{h}) \qquad (11)$$

where $z_k\mathbf{h} = i_k\mathbf{h} + \wp\mathbf{h}$, $\wp \in \mathbb{N}$, and $z_k\mathbf{h}$ presents the sampling instant among two adjacent instants. Using the *A-ETC method*, the next transmission moment may now be expressed as:

$$i_{k+1}\mathbf{h} = i_k\mathbf{h} + \min_{\wp\in\mathbb{N}}\{\wp\mathbf{h} \mid e_k^T(t)\Omega e_k(t) > \sqrt{\sigma}\mathbf{y}^T(i_k\mathbf{h})\Omega\mathbf{y}(i_k\mathbf{h}) \qquad (12)$$

$0 < \sigma < 1$ is a variable in the threshold, and $\Omega > 0$ is a weighting matrix for the triggering condition to be found. It is found that the forthcoming transmission moment is $i_{k+1}\mathbf{h}$ influenced by two variables. One is the trigger parameter, that will be determined by the *ETC-strategy*, and another is the system's output $\mathbf{y}(i_k\mathbf{h})$. It is obvious from (12) that the pair of transmitted instants may be represented as $\{i_k\mathbf{h} \mid i_k \in \mathbb{N}\}$, that provides the sampled instant as $\{i_k\mathbf{h} \mid i_k \in \mathbb{N}\}$, and the starting condition is $i_0\mathbf{h} = 0$. In this article, the channel induced delay by channel is represented by d_{i_k} and $d_{i_{k+1}}$ over the transmission instants $i_{k+1}\mathbf{h}$, respectively. Then, when the corresponding transmitted signal is at *zero-order-hold (ZOH)*, $i_k\mathbf{h} + d_{i_k}$ measure the instant.

We notice that $\breve{y}(t)$ preserves the value $\mathbf{y}(i_k\mathbf{h})$ with holding interval $\delta_{i_k} = [i_k\mathbf{h}+d_{i_k}, i_{k+1}\mathbf{h}+d_{i_{k+1}})$, under the effect of the *logic ZOH*.

$$\breve{y}(t) = \mathbf{y}(i_k\mathbf{h}), \quad t \in \delta_{i_k} \qquad (13)$$

In addition to the following subsets to designate the ZOH holding zone $\mho$ [43]:

$$\mho = [\; i_k\mathbf{h}+d_{i_k}, i_{k+1}\mathbf{h}+d_{i_{k+1}} \;) = \bigcup_{\wp=0}^{k_l}\mho_\wp \qquad (14)$$

where $\mho_\wp = [i_k\mathbf{h} + d_{i_k}, i_{k+1}\mathbf{h} + \mathbf{h} + d_{i_{k+1}})$, $\wp = 0, 1, 2, \cdots, k_l$, $k_l = i_{k+1} - i_k - 1$.

The network interruption is now defined $\eta(t) = t - i_k\mathbf{h}$, it obtains that $0 \le d_{i_k} \le \eta(t) \le \mathbf{h} + \bar{\tau} \equiv \eta_M$. Based on the aforementioned analysis, the initial input of the observer may be expressed as:

$$\breve{y}(t) = y(i_k\mathbf{h}) = y(t - \eta(t)) - e_k(t) \tag{15}$$

D. Observer-based Control design of MPPT using the stochastic T–S fuzzy

In the formation of observer-based control, we suppose that observer does retain the same premise membership function as it mention in the system (10), but, there is an existing communication channels. An observer with totally different assumptions will be computed first to evaluate the unmeasured states, and then a *PDC fuzzy controller* will be built for control requirements based on the estimated states.

The observer's rule is as follows, based on the previously described ETC-strategy and network induced time-varying delay.

Observer Rule j: **IF** $g_1(t)$ **is** W_j^1 **and** $\cdots g_\varrho(t)$ **is** W_j^ϱ **THEN**

$$\begin{cases} \dot{\hat{p}}(t) &= \mathcal{A}_j(\phi(t))\hat{p}(t)) + \mathcal{B}_j(\phi(t))u(t) + \mathcal{B}_{w_j}(\phi(t))\omega(t) \\ &+ \mathcal{L}_j(\breve{y}(t) - \hat{y}(t)) \\ \hat{y}(t) &= \mathcal{C}_j\hat{p}(t) \end{cases}$$

where $W_q^k(k = 1, 2, \cdots, \varrho, q = 1, 2, \cdots, j)$ represents the fuzzy set, $\hat{p}(t) \in \mathbf{R}^n$ denotes the observer sate, $\breve{y}(t) = \mathbf{y}(i_k\mathbf{h}) \in \mathbf{R}^m$ is the measured signal through ET mechanism for $t \in [i_k\mathbf{h} + d_{i_k}, i_{k+1}\mathbf{h} + d_{i_{k+1}}]$ and dignified output indicated by $\breve{y}(t) \in \mathbf{R}^m$. $\mathcal{L}_j$ is observer gain to be intended.

In terms of an global dynamics, the observer can be described as:

$$\begin{cases} \dot{\hat{p}}(t) &= \sum_{j=1}^r \hslash_j(g(t))[\mathcal{A}_j(\phi(t))\hat{p}(t)) + \mathcal{B}_j(\phi(t))u(t) \\ &+ \mathcal{B}_{w_j}(\phi(t))\omega(t) + \mathcal{L}_j(\breve{y}(t) - \hat{y}(t))] \\ \hat{y}(t) &= \sum_{j=1}^r \hslash_j(g(t))\mathcal{C}_j\hat{p}(t) \end{cases}$$

definition of premise variables and the membership are same as mentioned in eq. (8).

The observer and controller are connected directly in Fig. 1, and there is no network between them. As a result, the fuzzy controller and observer are considered to have the same premise variable. This observer-based late fuzzy control law is now determined.

Controller Rule m: IF $g_1(t)$ is W_1^m and $\cdots$ and $g_p(t)$ is W_p^m, THEN

$$u(t) = K_m(\phi(t))\hat{p}(t) \tag{16}$$

K_m stands for controller parameters that will be determined later. The fuzzy controller may thus be expressed as:

$$u(t) = \sum_{m=1}^r h_m(g(t))K_m(\phi(t))\hat{p}(t) \tag{17}$$

Remark 1: In this problem, fuzzy controllers are designed using the PDC control strategy. Controllers (17) and fuzzy systems (10) can have different membership functions. The flexibility of controller design is superior when compared to T-S fuzzy models with PDC control schemes. Despite this freedom of choice, the membership functions of the designed controller are still constrained as we will demonstrate in subsequent analyses. As long as Theorem 2 conditions were met, the membership functions of controllers in traditional PDC control schemes were usually arbitrarily defined. There is a general understanding that different selections of membership functions for controllers have varied effects on plants, such as anti-disturbance performance and convergence speed.

After calculating the estimation error using $\tilde{p}(t) \triangleq p(t) - \hat{p}(t)$, the observer error may be computed as follows:

$$\dot{\tilde{p}}(t) = \dot{p}(t) - \dot{\hat{p}}(t) \tag{18}$$

Furthermore, when we combine (16) and (18) at the same time, we obtain:

$$\begin{aligned} \dot{\tilde{p}}(t) &= \sum_{i=1}^r \sum_{j=1}^r \sum_{m=1}^s \hslash_i(g(t))\hslash_j(g(t))\hslash_m(g(t))[\mathcal{A}_i(\phi(t))(\tilde{p}(t)) \\ &+ \hat{p}(t) - \mathcal{A}_j(\phi(t))\hat{p}(t) + \mathcal{B}_i(\phi(t))\mathcal{K}_m(\phi(t)) - \mathcal{B}_j(\phi(t))\mathcal{K}_m \\ &(\phi(t))\hat{p}(t) + \mathcal{E}_0(\phi(t))p_b(t) - \mathcal{B}_{\omega_j}(\phi(t))\omega(t) \\ &- \mathcal{L}_j\mathcal{C}_i p(t - \eta(t)) + \mathcal{L}_j e_k(t) + \mathcal{L}_j\mathcal{C}_i p(t)] \end{aligned}$$

Denote the augmented vector $\zeta(t) = \begin{bmatrix} \hat{p}(t) \\ \tilde{p}(t) \end{bmatrix}$, then our augmented system becomes:

$$\begin{aligned} \dot{\zeta}(t) &= \sum_{i,j=1}^r \sum_{m=1}^s \hslash_i \hslash_j \hslash_m [\mathcal{A}_{ijm}\zeta(t) \\ &+ \mathcal{A}_{\eta ij}H\zeta(t - \eta(t)) + \mathcal{B}_w\tilde{\omega}(t) + \mathcal{L}_{e_j}e_k(t)] \end{aligned} \tag{19}$$

where

$$\mathcal{A}_{ijm} = \begin{bmatrix} \nu_1 & \mathcal{L}_j\mathcal{C}_i \\ \nu_2 & \mathcal{A}_i(\phi(t)) \end{bmatrix}, \quad \mathcal{A}_{\eta ij} = \begin{bmatrix} \mathcal{L}_j\mathcal{C}_i \\ -\mathcal{L}_j\mathcal{C}_i \end{bmatrix}$$

$$\mathcal{B}_w = \begin{bmatrix} 0 & \mathcal{B}_{\omega_j}(\phi(t)) \\ \mathcal{E}_0(\phi(t)) & -\mathcal{B}_{\omega_j}(\phi(t)) \end{bmatrix}, \quad \mathcal{L}_{e_j} = \begin{bmatrix} -\mathcal{L}_j \\ \mathcal{L}_j \end{bmatrix}$$

$$H = \begin{bmatrix} I & I \end{bmatrix}, \quad \tilde{\omega}(t) = \begin{bmatrix} p_b(t) \\ \omega(t) \end{bmatrix}$$

$$\nu_1 = \mathcal{A}_j(\phi(t)) + \mathcal{B}_j(\phi(t))\mathcal{K}_m(\phi(t)) - \mathcal{L}_j\mathcal{C}_i$$

$$\nu_2 = \mathcal{A}_i(\phi(t)) - \mathcal{A}_j(\phi(t)) - \mathcal{L}_j\mathcal{C}_i$$
$$+ (\mathcal{B}_i(\phi(t)) - \mathcal{B}_j(\phi(t)))\mathcal{K}_m(\phi(t))$$

PC generator's stochastic stability is examined in the following section.

IV. DESIGN ANALYSIS

We shall demonstrate the stochastic stability in the T–S fuzzy model of *PC* generating system with time–varying delays *NCSs* in the present section. Assume that a nonlinear system has time–varying delays that vary from system to system (19).

Theorem 1: Under the given condition of event-triggered scheme (12) with triggering parameter Ω, then resultant system (19) is stochastically stable for reasonable communication delay $\eta(t)$, if there exist matrices $\mathcal{P}_m > 0$, $\mathcal{Q}_m > 0$, $\mathcal{R}_m > 0$, $\mathcal{Z}_m > 0$, $\mathcal{S} > 0$,

$\mathcal{W} > 0$ and $\mathcal{Z}_m > 0$, so that

$$\mathbb{Q}_m = \sum_{m=1}^{s} \pi_{nm} (\mathcal{Q}_m + \mathcal{R}_m) - \mathcal{S} < 0 \qquad (20)$$

$$\mathbb{R}_m = \sum_{m=1}^{s} \pi_{nm} \mathcal{R}_m - \mathcal{S} < 0 \qquad (21)$$

$$\mathbb{Z}_m = \sum_{m=1}^{s} \pi_{nm} \mathcal{Z}_m - \eta_M^{-1} \mathcal{W} < 0 \qquad (22)$$

$$\begin{bmatrix} \mathcal{Z}_m & \mathcal{M}_m \\ \heartsuit & \mathcal{Z}_m \end{bmatrix} > 0 \qquad (23)$$

$$\Theta_{ijm} + \Theta_{jim} < 0, \quad i < j \in r, \quad m \in \mathcal{S} \qquad (24)$$

and the following inequalities hold:

$$\Theta_{ijm} =$$

$$\begin{bmatrix} \Theta_{ijm}^{11} & \Theta_{ijm}^{12} & \mathcal{M}_m & \mathcal{P}_m \mathcal{L}_{ej} \\ \heartsuit & \Theta_{ijm}^{22} & \Theta_{ijm}^{23} & 0 \\ \heartsuit & \heartsuit & \Theta_{ijm}^{33} & 0 \\ \heartsuit & \heartsuit & \heartsuit & -\sqrt{\sigma}\Omega \\ \heartsuit & \heartsuit & \heartsuit & \heartsuit \\ \heartsuit & \heartsuit & \heartsuit & \heartsuit \\ \heartsuit & \heartsuit & \heartsuit & \heartsuit \end{bmatrix}$$

$$\begin{bmatrix} \mathcal{P}_m \mathcal{B}_\omega & (\mathcal{P}_m \mathcal{A}_{ijm})^T & (\mathcal{P}_m \mathcal{C}_i)^T \\ 0 & (\mathcal{P}_m \mathcal{A}_{\eta ij})^T & 0 \\ 0 & 0 & 0 \\ 0 & (\mathcal{P}_m \mathcal{L}_{ej})^T & 0 \\ -\gamma^2 I & (\mathcal{P}_m \mathcal{B}_w)^T & 0 \\ \heartsuit & \Theta_{ijm}^{66} & 0 \\ \heartsuit & \heartsuit & -I \end{bmatrix}$$

where

$$\Theta_{ijm}^{11} = \sum_{m=1}^{s} \pi_{nm} \mathcal{P}_m + \mathcal{Q}_m + \mathcal{R}_m + \eta_M \mathcal{S} - \mathcal{Z}_m + \mathcal{P}_m \mathcal{A}_{ijm}$$

$$+ (\mathcal{P}_m \mathcal{A}_{ijm})^T, \quad \Theta_{ijm}^{12} = \mathcal{P}_m \mathcal{A}_{\eta ij} + \mathcal{Z}_m - \mathcal{M}_m$$

$$\Theta_{ijm}^{22} = (1 - \eta_M) \mathcal{Q}_m - 2\mathcal{Z}_m + \mathcal{M}_m$$

$$+ \mathcal{M}_m^T + H^T C_i^T \Omega C_i H$$

$$\Theta_{ijm}^{23} = \mathcal{Z}_m - \mathcal{M}_m, \quad \Theta_{ijm}^{33} = -\mathcal{R}_m + \mathcal{Z}_m$$

$$\Theta_{ijm}^{66} = (\eta_M^2 \mathcal{Z}_m + 1/2\eta_M{}^2 \mathcal{W}_m)$$

Proof: At this particular moment, the Lyapunov–Krasovskii function candidate for plant (19), is implemented.

$$\mathbb{V}(p_t, \phi(t)) = \zeta(t)^T \mathcal{P}(\phi(t)) \zeta(t) + \sum_{\ell=1}^{3} \mathbb{V}_\ell(p_t, \phi(t)) \qquad (25)$$

where

$$\mathbb{V}_1(p_t, \phi(t)) = \int_{t-\eta(t)}^{t} \zeta(v)^T \mathcal{Q}(\phi(t)) \zeta(v) dv$$

$$+ \int_{t-\eta_M}^{t} \zeta(v)^T \mathcal{R}(\phi(t)) \zeta(v) dv$$

$$\mathbb{V}_2(p_t, \phi(t)) = \eta_M \int_{-\eta_M}^{0} \int_{t+\beta}^{t} \dot{\zeta}(v)^T \mathcal{Z}(\phi(t)) \dot{\zeta}(v) dv d\beta$$

$$+ \int_{-\eta_M}^{0} \int_{t+\beta}^{t} \zeta(v)^T \mathcal{S} \zeta(v) dv d\beta$$

$$\mathbb{V}_3(p_t, \phi(t)) = \int_{-\eta_M}^{0} \int_{\theta}^{0} \int_{t+\beta}^{t} \dot{\zeta}(v)^T \mathcal{W} \dot{\zeta}(v) dv d\beta d\theta$$

where $\mathcal{P}(\phi(t)) > 0$, $\mathcal{Q}(\phi(t)) > 0$, $\mathcal{R}(\phi(t)) > 0$, $\mathcal{Z}(\phi(t)) > 0$, $\mathcal{S} > 0$, and $\mathcal{W} > 0$. Assume that $\mathbf{A}$ represents an infinitesimal weak generator of the process $\{p(t), \phi(t)\}$. Then, by implementing the same topologies as mentioned in [30], $\phi(t) = m \in \mathcal{S}$. To calculate this time derivative for $\mathbb{V}_\ell(p_t, \phi(t))$ $(\ell = 1, 2, 3)$ that solutions to (19) can be divided as:

$$\mathbf{A}\mathbb{V}(p_t, \phi(t))$$

$$= \zeta(t)^T \left(\sum_{m=1}^{s} \pi_{nm} \mathcal{P}_m + \mathcal{Q}_m + \mathcal{R}_m + \eta_M \mathcal{S} \right) \zeta(t)$$

$$+ 2\zeta(t)^T \mathcal{P}_m \dot{\zeta}(t) - \zeta(t - \eta_M)^T \mathcal{R}_m \zeta(t - \eta_M)$$

$$- (1 - \dot{\eta}(t)) \zeta(t - \eta(t))^T \mathcal{Q}_m \zeta(t - \eta(t))$$

$$- \dot{\zeta}(t)^T \left(\eta_M^2 \mathcal{Z}_m + 1/2\eta_M{}^2 \mathcal{W}_m \right) \dot{\zeta}(t)$$

$$- \eta_M \int_{t-\eta_M}^{t} \dot{\zeta}(v)^T \mathcal{Z}_{\ell i} \dot{\zeta}(v) dv$$

$$+ \int_{t-\eta(t)}^{t} \zeta(v)^T \mathbb{Q}_m \zeta(v) dv$$

$$+ \int_{t-\eta_M}^{t-\eta(t)} \zeta(v)^T \mathbb{R}_m \zeta(v) dv$$

$$+ \eta_M^- \int_{-\eta_M}^{0} \int_{t+\beta}^{t} \dot{\zeta}(v)^T \mathbb{Z}_m \dot{\zeta}(v) dv d\beta$$

To handle the inequalities in the above eqs., we have:

$$-\eta_M \int_{t-\eta_M}^{t} \dot{\zeta}(v)^T \mathbb{Z}_m \dot{\zeta}(v) dv \le$$

$$\sigma(t)^T \begin{bmatrix} -\mathcal{Z}_m & \mathcal{Z}_m - \mathcal{M}_m & \mathcal{M}_m \\ \heartsuit & -2\mathcal{Z}_m + \mathcal{M}_m + \mathcal{M}_m^T & \mathcal{Z}_m - \mathcal{M}_m \\ \heartsuit & \heartsuit & \mathcal{Z}_m \end{bmatrix} \sigma(t)$$

$$(26)$$

where

$$\sigma(t) = \begin{bmatrix} \zeta(t) \\ \zeta(t - \eta(t)) \\ \zeta(t - \eta_M) \end{bmatrix}$$

Recalling the triggering condition (12), $t \in [i_k \mathbf{h} + d_{i_k}, i_{k+1}\mathbf{h} + d_{i_{k+1}})$ we have:

$$e_k^T(i_k\mathbf{h})\Omega e_k(i_k\mathbf{h}) \leq \sqrt{\sigma} y(t - \eta(t))^T \Omega y(t - \eta(t)) \quad (27)$$

which is the same as

$$y(t - \eta(t))^T \Omega y(t - \eta(t)) = \zeta(t - \eta(t))^T H^T C_i^T \Omega C_i H \zeta(t - \eta(t))$$

Define the augmented matrix now

$$\xi(t) = col[\zeta(t), \zeta(t - \eta(t)), \zeta(t - \eta_M(t)), e_k(t), \tilde{\omega}(t)]$$

Integrating the (26)–(27) with event triggering mechanism (12), we get with the H_∞ performance index can be evaluated as:

$$\mathbf{A}\{\mathbb{V}(p_t, \phi(t))\} \quad - \quad \mathbf{A}\left(y(t)^T y(t) + \gamma^2 \tilde{\omega}(t)^T \tilde{\omega}(t)\right)$$

$$\leq \quad \xi^T(t)\Theta_{ijm}\xi(t) \quad (28)$$

Note that

$$\mathbb{Z}_m = \mathcal{P}_m[\mathcal{P}_m\mathbb{Z}_m^{-1}\mathcal{P}_m]\mathcal{P}_m \leq P_m[2\mathcal{P}_m - \mathbb{Z}_m]^{-1}\mathcal{P}_m$$

We can see that the matrix on the right–hand side of (28) is negative definite by applying the Schur complement, which indicates that $\Theta_{ijm} < 0$. This, along with (28), suggests that

$$\mathbf{A}\{\mathbb{V}(p_t, \phi(t))\} - \mathbf{A}\left(y(t)^T y(t) + \gamma^2 \tilde{\omega}(t)^T \tilde{\omega}(t)\right) \leq 0 \quad (29)$$

As a result, it is not difficult to show that the resultant system (19) is stochastically stable by following a similar path as in the proof of [30, Theorem 1]. As a result, the proof of this theorem is simple to accomplish. □

Theorem 2: Under the given condition of event-triggered scheme (12) with triggering parameter $\breve{\Omega}$, then resultant system (19) is stochastically stable for reasonable communication delay $\eta(t)$, if there exist matrices $\breve{\mathcal{X}}_m > 0$, $\breve{\mathcal{Q}}_m > 0$, $\breve{\mathcal{R}}_m > 0$, $\breve{\mathcal{Z}}_m > 0$, $\breve{\mathcal{S}} > 0$, $\breve{\mathcal{W}} > 0$, $\mathcal{Z}_m > 0$, and $\breve{\Omega}$ such that

$$\sum_{m=1}^{s} \pi_{nm}\left(\breve{\mathcal{Q}}_m + \breve{\mathcal{R}}_m\right) - \breve{\mathcal{S}} < 0 \quad (30)$$

$$\sum_{m=1}^{s} \pi_{nm}\breve{\mathcal{R}}_m - \breve{\mathcal{S}} < 0 \quad (31)$$

$$\sum_{m=1}^{s} \pi_{nm}\breve{\mathcal{Z}}_m - \eta_M^{-1}\breve{\mathcal{W}} < 0 \quad (32)$$

$$\begin{bmatrix} \breve{\mathcal{Z}}_m & \breve{\mathcal{M}}_m \\ \heartsuit & \breve{\mathcal{Z}}_m \end{bmatrix} > 0 \quad (33)$$

$$\breve{\Theta}_{ijm} + \breve{\Theta}_{jim} < 0, \quad i < j \in r, \quad m \in \mathcal{S} \quad (34)$$

and the following inequalities hold:

$$\breve{\Theta}_{ijm} = \quad = \quad \begin{bmatrix} \breve{\Theta}_{ijm}^{11} & \breve{\Theta}_{ijm}^{12} & \breve{\mathcal{M}}_m & \emptyset_{ijm_3} \\ \heartsuit & \Theta_{ijm}^{22} & \breve{\Theta}_{ijm}^{23} & 0 \\ \heartsuit & \heartsuit & \breve{\Theta}_{ijm}^{33} & 0 \\ \heartsuit & \heartsuit & \heartsuit & -\sqrt{\sigma}\Omega \\ \heartsuit & \heartsuit & \heartsuit & \heartsuit \\ \heartsuit & \heartsuit & \heartsuit & \heartsuit \\ \heartsuit & \heartsuit & \heartsuit & \heartsuit \end{bmatrix}$$

$$\begin{bmatrix} \emptyset_{ijm_4} & \emptyset_{ijm_1}^T & (\mathcal{P}_m\mathcal{C}_i)^T \\ 0 & \emptyset_{ijm_2}^T & 0 \\ 0 & 0 & 0 \\ 0 & \emptyset_{ijm_3}^T & 0 \\ -\gamma^2 I & \emptyset_{ijm_4}^T & 0 \\ \heartsuit & \breve{\Theta}_{ijm}^{66} & 0 \\ \heartsuit & \heartsuit & -I \end{bmatrix}$$

where

$$\breve{\Theta}_{ijm}^{11} = \sum_{m=1}^{s} \pi_{nm}X_m + \breve{\mathcal{Q}}_m + \breve{\mathcal{R}}_m + \eta_M\breve{\mathcal{S}} - \breve{\mathcal{Z}}_m$$

$$+ \quad \emptyset_{ijm_1} + \emptyset_{ijm_1}^T, \quad \breve{\Theta}_{ijm}^{12} = \emptyset_{ijnm_2} + \breve{\mathcal{Z}}_m - \breve{\mathcal{M}}_m$$

$$\breve{\Theta}_{ijm}^{22} = (1 - \eta_M)\breve{\mathcal{Q}}_m - 2\breve{\mathcal{Z}}_m + \breve{\mathcal{M}}_m$$

$$+\breve{\mathcal{M}}_m^T + H^T C_i^T \Omega C_i H$$

$$\breve{\Theta}_{ijm}^{23} = \breve{\mathcal{Z}}_m - \breve{\mathcal{M}}_m, \quad \breve{\Theta}_{ijm}^{33} = -\breve{\mathcal{R}}_m + \breve{\mathcal{Z}}_m$$

$$\breve{\Theta}_{ijm}^{66} = \left(\eta_M^2\breve{\mathcal{Z}}_m + 1/2\eta_M^2\breve{\mathcal{W}}_m\right)$$

$$\emptyset_{ijm_1} = \begin{bmatrix} \mathcal{A}_{jm}X_m + \mathcal{B}_j Y_j - \mathcal{F}_j\mathcal{C}_i \\ (A_{im} - A_{jm})X_j + (B_{im} - B_{jm})Y_j + \mathcal{F}_j\mathcal{C}_j \\ \\ \mathcal{F}_j\mathcal{C}_i \\ 0 \end{bmatrix}$$

$$\emptyset_{ijm_2} = \begin{bmatrix} \mathcal{F}_j\mathcal{C}_i \\ -\mathcal{F}_j\mathcal{C}_i \end{bmatrix} H, \quad \emptyset_{ijm_3} = \begin{bmatrix} -\mathcal{F}_j \\ \mathcal{F}_j \end{bmatrix}$$

$$\emptyset_{ijm_4} = \begin{bmatrix} 0 & 0 \\ \mathcal{E}_{0m}X_j & \mathcal{B}_{\omega_{jm}}X_j \end{bmatrix}$$

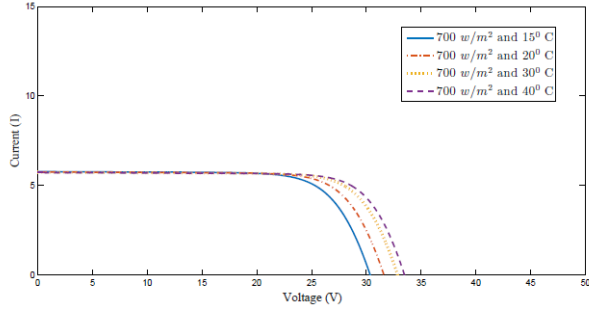The controller & observer gains for the *PC* generators are given as follows:

$$\mathcal{K}_m = Y_j X_m^{-1}, \quad \mathcal{L}_j = \mathcal{F}_j\mathbb{OS}X_m^{-1}\mathbb{S}^{-1}\mathbb{O}^{-1}. \quad (35)$$
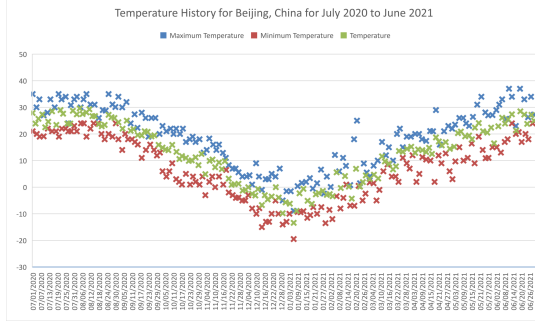
Proof: Suppose

$$\mathcal{P}_m = \begin{bmatrix} \mathcal{P}_i & \heartsuit \\ \heartsuit & \mathcal{P}_m \end{bmatrix}$$

$$X_m = \mathcal{P}_m^{-1}, \quad X_m\mathcal{Q}_mX_m = \breve{\mathcal{Q}}_m, \quad X_m\mathcal{R}_mX_m = \breve{\mathcal{R}}_m,$$

(a) P–V properties under same nominal ir-radiance ($\mathcal{Z} = 700 w/m^2$) of proposed $3.7kW$ panel with different temp. scenarios.

(b) Temperature record over 1 year for PC arrays.

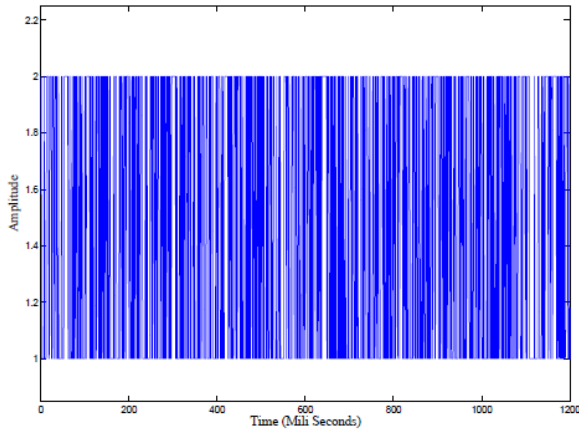Fig. 3: Feasibility for the *PC* generators n terms of temperature.

Fig. 4: Stochastic process for the load profile.

$$X_m \mathcal{Z}_m X_m = \check{\mathcal{Z}}_m, \quad X_m \mathcal{M}_m X_m = \check{\mathcal{M}}_m, \quad X_m \Omega X_m = \check{\Omega}.$$

For

$$X_m = V \begin{bmatrix} X_{1m} & \heartsuit \\ \heartsuit & X_{2m} \end{bmatrix} V^T$$

According to Lemma [30, Lemma 2], there exist $\tilde{X}_m = \mathbb{OS} X_{1m} \mathbb{S}^{-1} \mathbb{O}^{-1}$.

Let $\mathcal{C}_i X_m = \check{X}_m \mathcal{C}_i$ where $\check{X}_m^{-1} = \mathbb{OS} X_{1m}^{-1} \mathbb{S}^{-1} \mathbb{O}^{-1}$.

Pre- and post multiply to (24) by $\{X_m, X_m, X_m, X_m, I\}$ and its transpose, which yields to (34). The proof can be finished consequently. □

Remark 2: This problem will be further investigated carefully to improve the results. Specially, by implementing the robust control problem and switching control problem with adaptive event-triggered

scheme. On the other side, authors will examine the properties of *T-P model transformation* with different intelligent schemes. In this method, authors will modify the fuzzy rules to get effective results for different dynamics systems.

V. T-P MODEL WITH POLY-TOPIC REPRESENTATION

A poly-topic representation is constructed using the *T-P model* in this section, which includes the vertex matrices, the combination parameter χ and the error of representation $l_i, i = 1, 2, 3, 4$. The poly-topic representation is adjusted to take into account filter relaxation through rectification. Starting with W_χ, it is assumed that the stacked matrix is of the sum-product type as follows [38]:

$$W_\chi = \sum_{l_1=1}^{L_1} \sum_{l_2=1}^{L_2} \cdots \sum_{l_{q_x}=1}^{L_{q_x}} \left(\prod_{q=1}^{q_x} \chi_{q,l_q}(\psi_q(t)) \right) W_{l_1, l_2 \ldots l_{q_x}} \quad (36)$$

where $\psi_q(t), q = 1, 2, \ldots, q_x$, are the corresponding components of $\psi(t)$. For the arbitrary q and $\theta_q(t)$,

$$\chi_{q,l_q}(\psi_q(t)) \in \Upsilon_{L_q}, \quad l_q = 1, 2, \ldots, L_q \quad (37)$$

The T-P form of (36) can also be rewritten as:

$$\mathbf{W}_\chi = \mathbf{W} \bigotimes_{q=1}^{q_x} \chi_q(\psi_q(t)), \quad (38)$$

where

$$\chi_q(\psi_q(t)) = \begin{bmatrix} \chi_{q,1}(\psi_q(t)) & \chi_{q,2}(\psi_q(t)) & \cdots & \chi_{q,L_q}(\psi_q(t)) \end{bmatrix}$$

There are entries in L_q rows in the vector. There are vertices $W_{l_1 l_2 \ldots l_{q_x}}$ at the positions $l_1 l_2 \ldots l_{q_x}$, in the tensor $\mathbf{W}$.

$$W_{l_1 l_2 \ldots l_{q_x}} = \mathbf{W}(l_1, l_2, \ldots, l_n, :, :)$$

Considering all possible indices of each dimension is indicated by the symbol ":". After that, T–P model transformations, originally proposed by *Baranyi* [38], can be used to acquire an initial poly-topic representation. For the better understanding of the readers, we add the flow steps of T-P system for the better understanding for the researchers.

1. Calculate the matrix-valued function.
2. Perform an approximate *HOSVD*.
3. Normalize the *HOSVD* data.

A. T–P Model Transformation

In order to understand the *T-P model transformation*, it is first necessary to recall the steps that are involved.

1) **Sample the matrix-valued function**:

- Consider $\mathbb{D}$ as the linearization region.
- If g_{n,j_n}, where $j_n = 1, 2, \ldots, \mathcal{J}_n$ and $\psi_n^- = g_{n,1} \leq g_{n,2} \leq \cdots \leq g_{n,\mathcal{J}_n} = \psi_{q_x}^+$ are equally spaced, then divide the intervals $[\psi_n^-, \psi_n^+]$ at the $\mathcal{J}_n$ ticks.
- Next, sample all the grid points $\psi_{j_1 j_2 \ldots j_{q_x}}^s = (g_{1,j_1}, g_{2,j_1}, \ldots, g_{q_x, j_{q_x}})$, $1 \leq j_n \leq \mathcal{J}_n$, $n = 1, 2, \ldots, q_x$. with the matrix-valued $\mathbf{W}(\psi)$.
- Therefore, the sampled matrix $\mathbf{W}(\psi_{j_1 j_2 \ldots j_{q_x}}^s)$ should be stored in the tensor $\mathbf{W}^s \in \mathbb{R}^{\mathcal{J}_1 \times \mathcal{J}_2 \times \cdots \times \mathcal{J}_{q_x} \times O \times R}$ at the position $\mathcal{J}_1 \mathcal{J}_2 \ldots \mathcal{J}_{q_x}$.

2) **Perform an approximate HOSVD**:

HOSVD is applied to the tensor $\mathbf{W}^s$ from dimension 1 to dimension q_x. Every $\mathcal{K}_n$ with non-zero n-mode entries in singular value is retained in the *SVD* steps of the *HOSVD*. The approximate *HOSVD* of $\mathbf{W}^s$ is as follows:

$$\mathbf{W}^s \approx \hat{\mathbf{W}}^s = \hat{\mathbf{S}} \bigotimes_{n=1}^{q_x} \mathcal{U}_n, \tag{39}$$

where $\mathcal{U}_n$ and $\hat{\mathbf{S}}$, have proper dimensions and the value of $\hat{\mathbf{W}}^s$ can be approximated by $\mathbf{W}^s$.

3) **Normalize the HOSVD data**:

To fulfill the following *SN* and *NN* conditions, $\mathcal{U}_n$ must be transformed to $\tilde{\mathcal{U}}_n$:

$$\mathbf{NN} : \tilde{u}_{n,j_n,k_n} \geq \tag{40}$$

$$\mathbf{SN} : \widetilde{sum}(\tilde{\mathcal{U}}_n) = 1_{\mathcal{J}_n}$$

In this case, $s\tilde{u}m$ represents the row summation of a matrix. In terms of the result of the transformation between the *T-P model* and actual data, we can conclude:

$$\mathbf{W}^s \approx \hat{\mathbf{W}}^s = \tilde{\mathbf{S}} \bigotimes_{n=1}^{q_x} \tilde{u}_n, \tag{41}$$

where $\tilde{\mathbf{S}}$ is transformed from $\hat{\mathbf{S}}$ in (39). We can construct $\mathbf{W}^s$ by dividing the tensor-matrix product by the equation (41) and arrive at the following equation (42);

$$\mathbf{W}(\psi_{j_1 j_2 \dots j_{q_x}}^s) \approx \hat{\mathbf{S}}(j_1, j_2, \dots, j_{q_x}, :, :)$$

$$= \tilde{\mathbf{S}} \bigotimes_{n=1}^{q_x} \tilde{u}_{n,j_n}$$

$$= \sum_{l_1=1}^{L_1} \sum_{l_2=1}^{L_2} \cdots \sum_{l_{q_x}=1}^{L_{q_x}} \prod_{n=1}^{q_x} \tilde{u}_{n,j_n,l_n} \tilde{\mathbf{S}}(l_1, l_2, \dots,$$

$$l_{q_x}, :, :), \tag{42}$$

where $\tilde{u}_{n,j_n}$ and $\tilde{u}_{n,j_n,k_N}$ are the j_n-th row vector and the $(j_n.l_N)$-th entry of $\tilde{\mathcal{U}}_n$, respectively.

Thus, the vertices $\mathbf{W}_{l_1 l_2 \dots l_{q_x}}$ are defined by $\tilde{S}(l_1, l_2, \dots, l_{q_x}, :, :)$, considering all possible scenarios of $l_1, l_2, \dots, l_{q_x}$. As a matter of fact that $\chi_{n,l_n}(g_{n,j_n})$, since $\tilde{\mathcal{U}}_n$ fulfills the *NN* and *SN* conditions. For the purpose of acquiring values of $\chi_n(\psi_n(t))$ for all $\psi_n \in [\psi_n^-, \psi_n^+]$, a linear interpolation is adopted to calculate the values of $\chi_n(\psi_n(t))$ between sample ticks. Using the maximum Frobenius norms of the sampled matrices $\mathbf{W}(\psi) - \mathbf{W}_\chi$, we can numerically compute the representation error l_i, $i = 1, 2, 4, 5$. The *T-P model transformation* leads to the acquisition of a polytopic representation candidate.

There is no dedicated representation for the filter problem in the *T-P model transformation*, which is only a general polytopic representation. As a result, conservatism will still be prevalent to a large degree. In some cases, vertex systems may be infeasible, so filter optimization is impossible (or in other words, conservativeness is infinitely large). By relaxing filter conservatism, we will rectify the *T-P model transformation* result in this subsection. To minimize representation error and ensure low conservatism in filter design, both vertex polytope $\mathbb{W}_c$ and vertex polytope $\mathbb{W}_c$ should be kept small. Retaining singular values makes it easy to adjust the representation error. The polytope bound pertaining to $\mathbb{W}$ becomes tighter with smaller vertex poly-topes $\mathbb{M}_c$. Therefore, $\hat{\mathbf{W}}^s$ and $\tilde{\mathbf{S}}$ have as many equal sub-matrices as they can. It also means that there are more *1-dominant* vectors with maximum entries extremely close to 1 in $\tilde{\mathcal{U}}_n$. The *SN* and *NN* matrices can be transformed into each other using the following lemma. Therefore, it will provide a method for

manipulating *SN*, *NN*, and *T–P matrix* elements, and for rectifying the results of *T–P model transformation*.

A unit vector is obviously 1-predominant when some of the points $\{t_j\}$ are exactly from $\{u_i\}$. The i_1^{th} row of $\mathcal{U}'$ will contain $\mathbb{L}_{e_{j1}}^{(n)}$ if the point t_{j1} is identical to u_{i1}, as shown below:

$$\mathbb{L}e_{j1}^{(n)} = [\ \underbrace{\overbrace{0 \quad 0 \quad \dots \quad 0 \quad 1}^{j1} \quad 0 \quad \dots \quad 0}_{n} \ ] \tag{43}$$

As a result of transforming $\tilde{\mathcal{U}}_n \in \mathbb{R}^{\mathcal{J}_n \times \mathcal{L}_n}$ into a matrix with more one-predominant row vectors, a tighter $\mathcal{K}_n$ vertex hyper-polytope is explored, encompassing the $\mathcal{J}_n$ points defined by $\tilde{\mathcal{U}}_n$ rows. $\mathcal{J}_n$ points have a convex hull which can be operated on by this procedure. The convex hull of the points $\tilde{\mathcal{U}}_n \in \mathbb{R}^{\mathcal{J}_n \times \mathcal{K}_n}$ is obtained by multiplying $\tilde{u}_{n,j}^T$, $j = 1, 2, \dots, \mathcal{J}_n$ by the rows in (41). As $\tilde{\mathcal{U}}_n$ is full column rank, the convex hull contains at least $\mathcal{K}_n$ points. A convex hull is bound exactly when the number of vertices equals $\mathcal{K}_n$. It would then be necessary for $\{\tilde{u}_{n,j}\}$ to have more than one $\mathcal{K}_n$–vertex polytope bound. To verify that each $\mathcal{K}_n$ -vertex polytope encircles all possible points $\{\tilde{u}_{n,j}\}$, we choose $\mathcal{K}_n$ "facets" from the convex hull. It follows that if it does, a $\mathcal{K}_n$–vertex polytope bound for $\{\tilde{u}_{n,j}\}$ is found, and the vertices of the polytope bound are exactly the intersection points of the selected "facets." Relieve the $\tilde{\mathcal{U}}_n$ and $\tilde{S}$ so that they are both equal to the $\mathcal{K}_n$-vertex of the polytope bound by $p_{n,i} \in \mathbb{R}^{\mathcal{K}_n \times 1}$, $i = 1, 2, \dots, \mathcal{K}_n$:

$$\bar{\mathcal{U}}_n = \tilde{\mathcal{U}}_n \Xi_{n,4}^{-1}, \quad n = 1, 2, \dots, q_x$$

$$\bar{\mathbf{S}} = \tilde{\mathbf{S}} \bigotimes_{n=1}^{q_x} \Xi_{n,4} \tag{44}$$

where $\Xi_{n,4} = [p_{n,1} \quad p_{n,2} \quad \dots \quad p_{n,\mathcal{K}_n}]^T$. To conclude, here are the following:

$$\mathbf{W}^s \approx \hat{\mathbf{W}}^s = \bar{\mathbf{S}} \bigotimes_{n=1}^{q_x} \bar{\mathcal{U}}_n, \tag{45}$$

You should continue to search for different types of $\Xi_{n,4}$, $n = 1, 2, \dots, q_x$ and perform the computations of (44) and (45) until you obtain a polytopic representation with tight vertex poly–topes that is satisfactory.

VI. RESULT AND DISCUSSION

In this portion, we present two examples of the benefits and merits of the designed algorithm here.

Example 1: In a computer simulation of a truck-trailer system with time-varying delay, the proposed design method will be implemented to backup control. Our vehicle-trailer model is designed to have time-varying delays, as shown below.

$$\begin{cases} \dot{p}_1(t) &= -b\frac{v\bar{i}}{Li_0}p_1(t) + \frac{v\bar{i}}{li_0}\mathsf{u}(t) - (1-b)\frac{v\bar{i}}{Li_0}p_1(t-\eta(t)) \\ \dot{p}_2(t) &= b\frac{v\bar{i}}{Li_0}p_1(t) + (1-b)\frac{v\bar{i}}{Li_0}p_1(t-\eta(t)) \\ \dot{p}_3(t) &= \frac{v\bar{i}}{i_0}\sin\left[p_2(t) + b\frac{v\bar{i}}{2L}p_1(t) + (1-b)\frac{v\bar{i}}{2L}p_1(t-\eta(t))\right] \end{cases}$$

where the angle difference between truck and trailer is presented by $p_1(t)$; $p_2(t)$ is denoted by trailer's angle; and $p_3(t)$ the vertical position of the trailer's rear end is expressed. The numerical values of
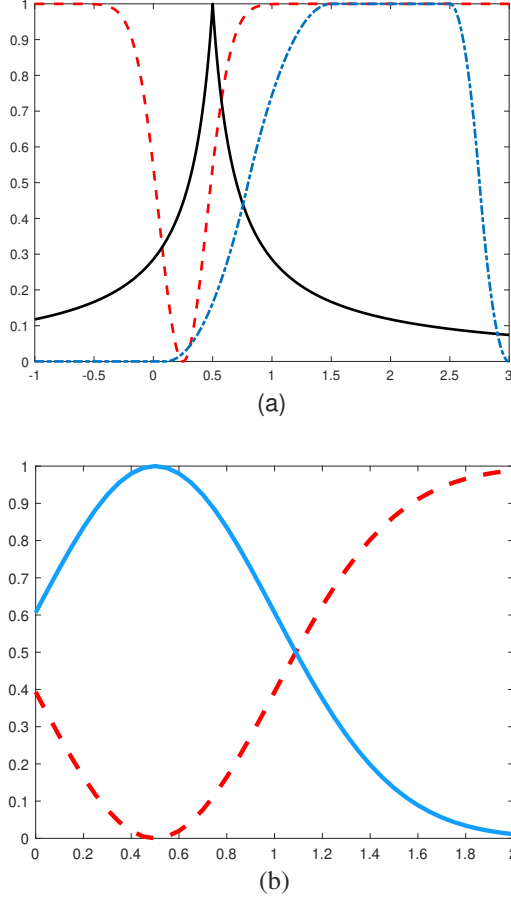
Fig. 5: Curves of convex combination coefficients given by $\bar{\mathcal{U}}_1$ and $\bar{\mathcal{U}}_2$ with (a) $p_1(t)$ and (b) $\phi(t)$, respectively.

$b, i, \bar{i}, L$ and v can be seen in [Table 1, [37]]. Due to the limitations of the pages, we omitted some mathematical steps.

$$\dot{p}(t) = \sum_{i=1}^{2}\sum_{j=1}^{2} \hbar_i(g(t))h_j(g(t)) \sum_{m=1}^{2} \lambda_m(g(t))[\mathcal{A}_i p(t)$$

$$+ \quad \mathcal{B}_i u(t) + \mathcal{B}_{\omega_j}(\phi(t))\omega(t)]$$

$$y(t) = \sum_{i=1}^{2}\sum_{j=1}^{2} \hbar_i(g(t))h_j(g(t)) \sum_{m=1}^{2} \lambda_m(g(t))\mathcal{C}_i p(t)$$

The membership functions for the T-S fuzzy system are as follows:

$$\begin{cases} h_1(t) = exp\left[-\frac{(p_1(t)-30)^2}{2\times 36^2}\right], & h_2(t) = 1 - h_1(t) \\ \hbar_1(t) = exp\left[-\frac{(p_1(t)-1.5)^2}{2\times 15^2}\right], & \hbar_2(t) = 1 - \hbar_1(t) \\ \lambda_1(t) = \frac{1}{1+exp[40(\phi(t)-1.5)]}, & \lambda_2(t) = 1 - \lambda_1(t) \end{cases}$$

With the first component of $\phi(t)$ representing a switch signal, and $\phi(t)$ representing a signal with a random value, $p_1(t)$ represents the first component of $p(t)$. Fig. 4 shows an example of the switching signal. In the domain $\mathbb{D}$, sampling ticks g_{n,j_n} are uniformly spaced with sampling rate, and the domain $\mathbb{D}$ is given as $\begin{bmatrix} -1 & 3 \end{bmatrix} \times \begin{bmatrix} 0 & 2 \end{bmatrix}$. As a result of the *HOSVD* routine in T-P model, the first three largest 1-mode (singular based values) and the first two largest

2-mode (singular based values) are retained. A column of $\mathcal{U}_1$ and $\mathcal{U}_2$ are represented by each curve in Figure 5.

To show the superiority of our proposed method, we made a comparison which is given in Table III. In this comparison, we obtained the optimal value of γ with different values of η_M. From Table III, it can be seen that our proposed methodology is less conservative as compared to [44].

TABLE III: Comparison of Minimum value γ performance index with different values of η_M.

η_M	0.1	0.25	0.40	0.65	0.95
[44]	0.1565	0.2532	0.2942	0.2193	0.2381
Theorem 2	10^{-3}	10^{-3}	10^{-2}	10^{-2}	10^{-1}

Vertices are defined as follows:

$$\begin{bmatrix} \bar{\mathbf{S}}(1,1,:,:) \\ \bar{\mathbf{S}}(1,2,:,:) \end{bmatrix} = \begin{bmatrix} -2.3750 & -0.3601 & 0.2401 & 0.3824 \\ 0.4975 & -2.6151 & 0.2401 & 0.5074 \\ -0.2401 & 0.0025 & -2.0174 & 0.6200 \\ 1.3700 & 0.8775 & 1.5248 & 0.2525 \\ \hline -2.8776 & -0.0026 & 0.1276 & 0.6224 \\ 0.3316 & -1.9158 & 0.0869 & 0.5790 \\ -0.1303 & 0.0816 & -2.6580 & 0.6684 \\ 1.2500 & 0.9131 & 2.0790 & 0.2934 \end{bmatrix}$$

$$\begin{bmatrix} \bar{\mathbf{S}}(2,1,:,:) \\ \bar{\mathbf{S}}(2,2,:,:) \end{bmatrix} = \begin{bmatrix} -2.3750 & -0.3749 & 0.2499 & 0.3751 \\ 0.5000 & -2.6249 & 0.2499 & 0.5001 \\ -0.2499 & 0 & -2.0003 & 0.6250 \\ 1.3750 & 0.8750 & 1.5002 & 0.2500 \\ \hline -2.8902 & -0.0153 & 0.1402 & 0.6098 \\ 0.3232 & -1.9116 & 0.1036 & 0.5580 \\ -0.1554 & 0.0732 & -2.6160 & 0.6767 \\ 1.2500 & 0.8964 & 2.0580 & 0.3018 \end{bmatrix}$$

$$\begin{bmatrix} \bar{\mathbf{S}}(3,1,:,:) \\ \bar{\mathbf{S}}(3,2,:,:) \end{bmatrix} = \begin{bmatrix} -2.3750 & -0.3750 & 0.2500 & 0.3750 \\ 0.5000 & -2.6250 & 0.2500 & 0.5000 \\ -0.2500 & 0 & -2.0000 & 0.6250 \\ 1.3750 & 0.8750 & 1.5000 & 0.2500 \\ \hline -2.9021 & -0.0271 & 0.1521 & 0.5979 \\ 0.3152 & -1.9076 & 0.1195 & 0.5381 \\ -0.1792 & 0.0653 & -2.5762 & 0.6847 \\ 1.2500 & 0.8805 & 2.0381 & 0.3097 \end{bmatrix}$$

In addition, we also implement the *T-P Model* for our system and compare it to traditional feedback control. Figure 6 shows the controller's results. A look at this figure illustrates the superiority of the proposed controller to the traditional one.

Example 2: This part explains how *Theorem 2* may be applied to *PC* generator systems. The information shown in this part was derived from a simulation that was given real-time weather data. In order to make the simulation as realistic as possible, we put the features of the Siemens solar module *SP75* in the simulator. Table II contains the entire specification for the *PC* generator. The simulations were run with the *PC* generator supplying a set of loads with varying power needs, which could be turned on and off at any time using a Markov chain. Three loads were taken into account. We have eight possibilities corresponding to eight modes of the Markov chain ϕ_t since each load may be turned on or off.

Fig. 3 depicts the *PC* power controller's overall structure. The *MPPT* searching block creates the trajectory shown in Figure 7–9 in order to get the maximum power accessible within the *PC* module. For this, we select the initial conditions $p(t) = \begin{bmatrix} 5 \\ -5 \\ -3 \end{bmatrix}$ with $\eta_M = 0.15$.
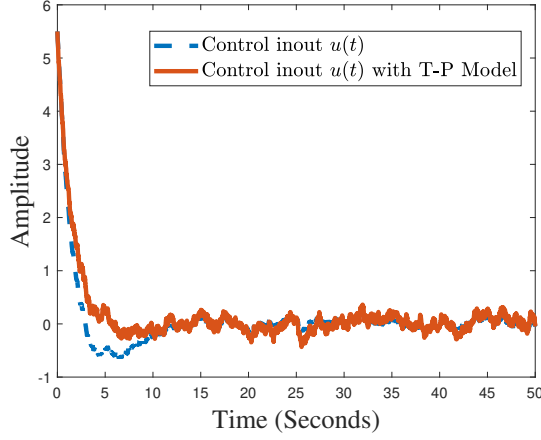
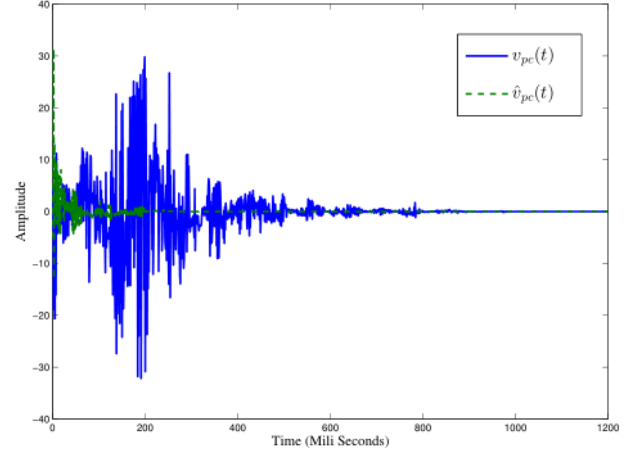Fig. 6: Control input with T-P model transformation.

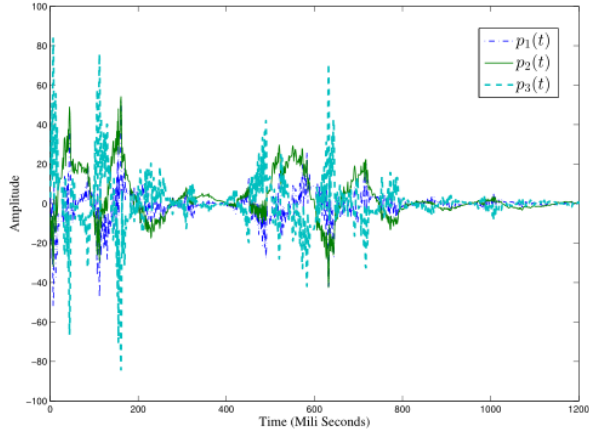Fig. 8: State trajectory of output voltage and its estimation.

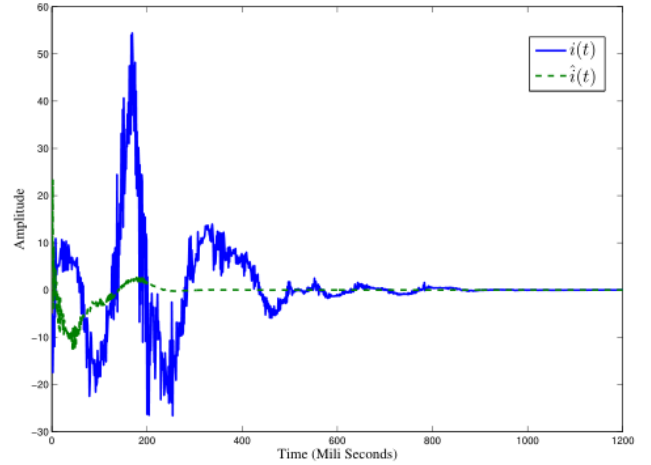Fig. 7: State trajectories for the closed–loop system.

Fig. 9: State trajectory of inductor current voltage and its estimation.

Let's select the continuous stochastic process for the load profile of the *PC* generators:

$$\pi_{nm} = \begin{bmatrix} -0.85 & 1.25 & -0.4 \\ 0.46 & -0.84 & 0.38 \\ 0.25 & 0.35 & -0.6 \end{bmatrix}$$

The LMIs (30)–(34) are then shown to be viable in the appropriate triggering matrix $\tilde{\Omega} = 5.841$, in the controller and observer gains for that *LMIs* are found to be valid as follows:

$$\begin{bmatrix} \mathcal{K}_1 \\ \mathcal{K}_2 \end{bmatrix} = \begin{bmatrix} 1.9817 & -0.7056 & 0.0337 \\ 1.1264 & -0.2209 & 0.0142 \end{bmatrix}$$

$$\begin{bmatrix} \mathcal{L}_1 \\ \mathcal{L}_2 \end{bmatrix}^T = \begin{bmatrix} -0.2130 & 1.7235 & -0.5175 \\ -0.4168 & -0.5176 & -1.5719 \end{bmatrix}^T$$

The power profile and load jumps in this simulation shadowed the sample route illustrated in Fig. 7. The closed–loop for the *PC* generator is depicted in Fig. 8. The state trajectories and their estimation are shown in 9–10, while in Fig. 9, we present the control input for the *PC* generator. Fig. 12, displays the communication instants and the communication intervals. From the above analysis, the *PC* generator produced a steady response, which we can determine from the simulated data, validating *Theorem 2's* result.

To conclude, the simulation for the *PC* generator shows that *Theorem 2's* stochastic *MPPT* control is effective in dealing with not just
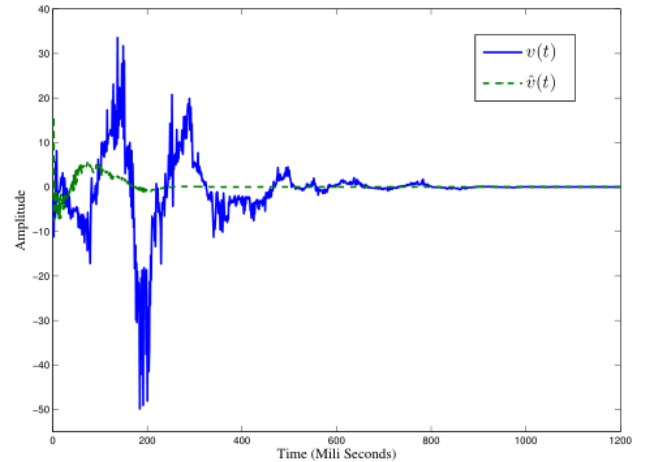

Fig. 10: State trajectory of capacitor voltage and its estimation.

random load variations but also changing environmental conditions. This feature demonstrates *Theorem 2's* application possibilities.
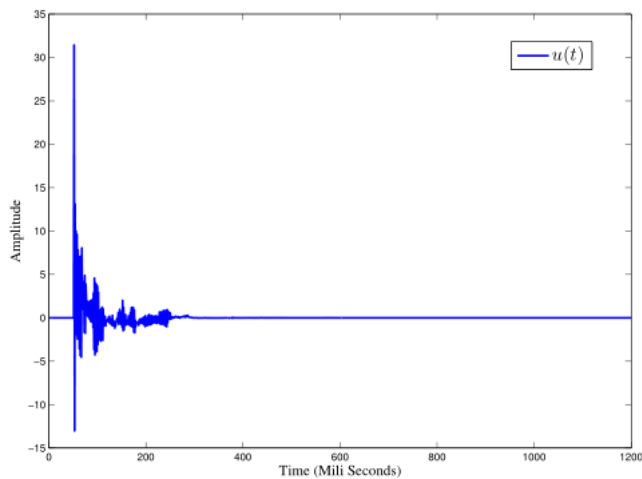
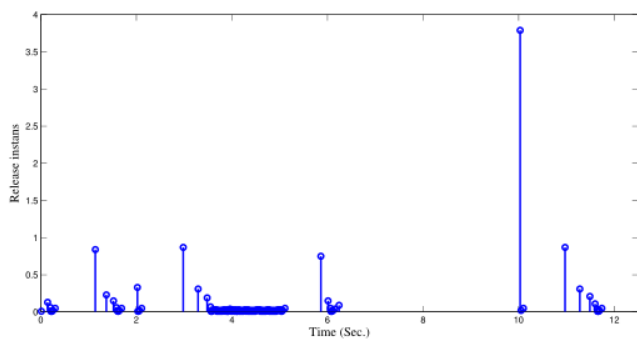Fig. 11: Behaviour of the control input.

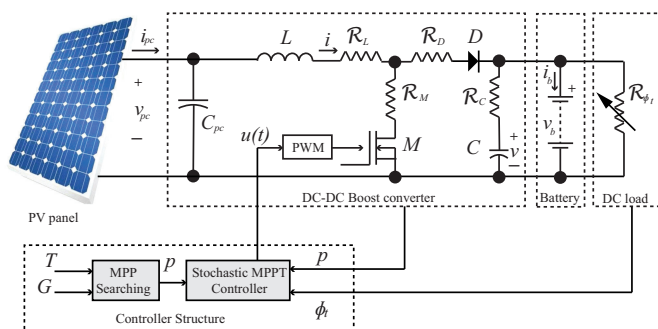Fig. 12: Release instants and release interval by event-triggered scheme.

Fig. 13: Circuit chart of solar panel.

Remark 3: An important point to emphasize is that the threshold value of the trigger condition strongly influences the control task's execution. Furthermore, since a threshold value in traditional design is a scalar, it is difficult to adapt to changes in the operating system, i.e., the event-triggered parameter is meant to react to external perturbations. Another way to achieve the triggering parameter would be via online optimization, which is a challenging process. Furthermore, pure-feedback systems are recognized to have an additional representational form rather than strict-feedback systems, that don't have an affine presence for this state variable shall be utilized as a powerful design controller. Thus, the controller design for pure-

feedback systems has pretty challenging, whereas the controller design for the debated system is simple to improve owing to the characteristics of the hybrid system. This is a gain from this projected effort. In addition Fig. 3 reveals the feasibility of our proposed method. Increasing temperature affects the performance of the *PC generators* (data available freely [1]. From the temperature analysis in Fig. 3a, it can easily see that the proposed algorithm can be implemented in the specified region.

Remark 4: Nonlinear models can be used to model photovoltaic generators, but they can be challenging to compute numerically. In place of dealing directly with the nonlinear plant, we have turned it into a T–S fuzzy plant that is numerically tractable. Our next step is to associate the model with loads driven by a Markov process, that we have studied in real-world scenarios. In order to account for the uncertainty in the weather data, we have developed our system.

VII. CONCLUSIONS

Nonlinear models may be used to describe solar generators, which can be challenging to deal with numerically. We transformed the nonlinear model into a T-S fuzzy model, which are more numerically tractable. This model was then affiliated to loads focused by a Markov chain, which is inspired by real-world application scenarios. This article's major aim was to provide a unique stochastic control for *MPPT* of solar producers utilizing observer-based control in a networked control environment. Our *ETC* system was developed to address the issue of bandwidth consumption. Conditions are the context for a proposed delayed observer–based fuzzy controller, that was accessible in the format of generic matrix *LMIs*, were acquired for the strength and performance study in these nonlinear systems. According to these simulation results, the controlled *PC* generator stayed steady and drew the maximum amount of power from the appropriate *PC* panel. To achieve tight vertex poly-topes and small representation form, two separate steps are developed in order to obtain an accurate representation of the plants. To adjust the vertex poly-tope, a specific rectifying procedure is developed in the second step using the *T-P model* transformation to obtain the candidate with the required representation. *Theorem 2's* potential for *photovoltaic cell (PC)* generators is demonstrated by this simulation-based evidence.

In the future, this problem further carefully studied to improve the efficiency of *MPPT* control design. For this, the control structure is given in Fig. 13.

REFERENCES

[1] C.A.S. Hall, K. Klitgaard. Energy and the Wealth of Nations: An Introduction to Biophysical Economics, *Springer International Publishing: Berlin/Heidelberg, Germany*, 2018.

[2] G. Kavari, M. Tahani, M. Mirhosseini. Wind shear effect on aerodynamicperformance and energy production of horizontal axis wind turbines withdeveloping blade element momentum theory, *Journal of Cleaner Production*, vol. 219, pp: 368–376, 2019.

[3] R.M. Elavarasan, S. Afridhis, R.R. Vijayaraghavan, U. Subramaniam, M. Nurunnabi. SWOT analysis : a framework for comprehensive evaluation of driversand barriers for renewable energy development in significant countries, *Energy Reports*, vol. 6, pp: 1838–1864, 2020.

[4] L. Ovalle, H. Ríos, H. Ahmed. Robust Control for an Active Suspension System via Continuous Sliding–Mode Controllers, *Engineering Science and Technology, an International Journal*, https://doi.org/10.1016/j.jestch.2021.06.006, 2021.

[5] M. Zare, F. Pazooki, S. E. Haghighi. Hybrid controller of Lyapunov–based and nonlinear fuzzy–sliding mode for a quadrotor slung load system, *Engineering Science and Technology, an International Journal*, https://doi.org/10.1016/j.jestch.2021.07.001, 2021.

[6] P. G. V. Sampaio, M. O. A. Gonzalez, R. M. de Vasconcelos, M. A. T. dos Santos, J.C. de Toledo, J.P.P. Pereira. Photovoltaic technologies: Mapping from patentanalysis, Renewable and Sustainable, *Energy Reviews*, vol. 93, pp: 215–224, 2018.

[7] G. M. Vargas Gil, R. BittencourtAguiar Cunha, S. Giuseppe Di Santo, R. MachadoMonaro, F. Fragoso Costa, A. J. SguareziFilho. Photovoltaic energy in South America: Current state and grid regulation for large-scale and distributed photovoltaicsystems, *Renewable Energy*, vol. 162, pp: 1307–1320, 2020.

[8] A. McEvoy, T. Markvart, L. Castanerr. Practical Handbook of Photovoltaics:Fundamentals and Applications, *Elsevier*, 2012.

[9] Y. Thiaux, T.T. Dang, L. Schmerber, B. Multon, H.B. Ahmed, S. Bacha, Q.T. Tran,Demand–side management strategy in stand–alone hybrid photovoltaic systems withreal–time simulation of stochastic electricity consumption behavior, *Applied Energy*, vol. 253, 113530, 2019.

[10] A. Jubaer, S. Zainal. An enhanced adaptive P&O MPPT for fast and efficient trackingunder varying environmental conditions, *IEEE Transactions on Sustainable Energy*, vol. 9, no. 3, pp: 1487–1496, 2018.

[11] A. Laib, F. Krim, B. Talbi, A. Kihal, H. Feroura. Improvedcontrol for three phase dual–stage grid-connected PV systemsbased on predictive control strategy, *Journal Control of Engineering and Applied Informatics*, vol. 20, no. 3, pp: 12–23, 2018.

[12] N. Priyadarshi, F. Azam, A. K. Bhoi, and A. K. Sharma. Dynamicoperation of grid-connected photovoltaic power system, *In Advances in Greener Energy Technologies. Singapore: Springer*, pp: 211–218, 2020.

[13] D. Sera, L. Mathe, T. Kerekes, S.V. Spataru, and R. Teodorescu. On the Perturb–and–Observe and incremental conductance MPPT methods for PV systems, *IEEE Journal of Photovoltaics*, vol. 3, no. 3, pp: 1070–1078, 2013.

[14] B. Subudhi and R. Pradhan. A comparative study on maximum power-point tracking techniques for photovoltaic power systems, *IEEE Transactions on Sustainable Energy*, vol. 4, no. 1, pp: 89–98, 2013.

[15] A. K. Podder, N. K. Roy, and H. R. Pota. MPPT methods for solar PVsystems: A critical review based on tracking nature, *IET Renewable Power Genereration*, vol. 13, no. 10, pp: 1615–1632, 2019.

[16] Y.H. Liu, J.H. Chen, J.W. Huang. A review of maximum powerpoint tracking techniques for use in partially shaded conditions, *Renewable and Sustainable Energy Reviews*, vol. 41, pp: 436–453, 2015.

[17] B. Yang, T. Zhu, J. Wang, H. Shu, T. Yu, X. Zhang, W. Yao, and L. Sun. Comprehensive overview of maximum power point tracking algorithmsof PV systems under partial shading condition, *Journal of Cleaner Production*, vol. 268,Art. no. 121983, 2020.

[18] S. Issaadi, W. Issaadi, A. Khireddine. New intelligent control strategy by robust neuralnetwork algorithm for real time detection of an optimized maximum power trackingcontrol in photovoltaic systems, *Energy*, vol.187, 115881, 2019.

[19] H. Khabou, M. Souissi, A. Aitouche. MPPT implementation on boost converter byusing T–S fuzzy method, *Mathematics and Computers in Simulation*, vol. 167, pp: 119–134, 2020.

[20] A. Riaz, A. F. Murtaza, H. A. Sher, Power tracking techniques for efficient operation ofphotovoltaic array in solar applications–A review, *Renewable and Sustainable Energy Reviews*, vol. 101, pp: 82–102, 2019.

[21] W.J. Wang, V.P. Vu, W. Chang, C.H. Sun, S.J. Yeh. A synthesisof observer-based controller for stabilizing uncertain T–S fuzzy systems, *Journal of Intelligent Fuzzy Systems*, vol. 30, no. 6, pp: 3451–3463, 2016.

[22] M. Sitbon, S. Schacham, A. Kuperman. Disturbance Observer–Based Voltage Regulation of Current–Mode–Boost–Converter–Interfaced Photovoltaic Generator, *IEEE Transactions on Industrial Electronics*, vol, 62, no. 9, pp: 5776–5785, 2015.

[23] K. Khayati. Multivariable Adaptive Sliding–Mode Observer–Based Control for Mechanical Systems. *Canadian Journal of Electrical and Computer Engineering*, vol. 38, no. 3, pp: 253–265, 2015.

[24] B. He, G. Liu, H. Chen, X. Hu. Extended state observer–based sliding mode learning control for mechanical system, *Measurement and Control*, pp: 1–9, 2020.

[25] J. Chen, R. Sun, B. Zhu. Disturbance observer–based control for small nonlinear UAV systems with transient performance constraint, *Aerospace Science and Technology*, vol. 105, 106028, 2020.

[26] R. Priem, N. Bertoli, Y. Diouane, A. Sgueglia. Upper trust bound feasibility criterion for mixed constrained Bayesian optimization with application to aircraft design, *Aerospace Science and Technology*, vol. 105, 105980, 2020.

[27] R. A. Lope, E. N. Tec–Caama, M. I. Neria–Gonzalez. Observer–Based Control for Uncertain Nonlinear Systems Applied to Continuous Biochemical Reactors, *Mathematical Problems in Engineering*, vol. 2020, Article ID: 6417860 , 2020.

[28] J. Sun and Z. Zeng. Periodic Event–Triggered Control for Networked Control Systems With External Disturbance and Input and Output Delays, *IEEE Transactions on Cybernetics*, doi: 10.1109/TCYB.2022.3164214, 2022.

[29] Z. Li, H. Yan, H. Zhang, S. X. Yang and M. Chen. Novel Extended State Observer Design for Uncertain Nonlinear Systems via Refined Dynamic Event–Triggered Communication Protocol, *IEEE Transactions on Cybernetics*, doi: 10.1109/TCYB.2022.3161271, 2022.

[30] M.S. Aslam, Z. Chen. Observer–based dissipative output feedback control for network T–S fuzzy systems under time delays with mismatch premise, *Nonlinear Dynamics*, vol. 95, pp: 2923–2941, 2019.

[31] M. A. G. de Brito, L. Galotto, L. P. Sampaio, G. d. A. e Melo, C. A. Canesin, Evaluation of the main MPPT techniques for photovoltaic applications, *IEEE Transactions on Industrial Electronics*, vol. 60, no. 3, pp: 1156–1167, 2013.

[32] N. Yildiran, E. Tacer, Identification of photovoltaic cell single diode discrete model parameters based on datasheet values, *Solar Energy*, vol. 127, pp: 175–183, 2016.

[33] W. Shinong, M. Qianlong, X. Jie, G. Yuan, L. Shilin, An improved mathematical model of photovoltaic cells based on datasheet information, *Solar Energy*, vol. 199, pp: 437–446 2020.

[34] M. Aatabe, F. E. l Guezar, A. N. Vargas, H. Bouzahir. A novel stochastic maximum power point tracking control for off-grid standalone photovoltaic systems with unpredictable load demand, *Energy*, vol. 235, 121272, 2021.

[35] Y. Thiaux, T. T. Dang, L. Schmerber, B. Multon, H. B. Ahmed, S. Bacha, Q. T. Tran. Demand–side management strategy in stand–alone hybrid photovoltaic systems with real-time simulation of stochastic electricity consumption behavior, *Applied Energy*, vol. 253, 113530, 2019.

[36] M. Aatabe, F. El Guezar, H. Bouzahir, A. N. Vargas. Constrained stochastic control of positive Takagi–Sugeno fuzzy systems with Markov jumps and its application to a DC–DC boost converter, *Transactions of the Institute of Measurement and Control*, vol. 42, no. 16, pp: 3234–3242, 2020.

[37] M.S. Aslam. L_2–L_∞ Control for Delayed Singular Markov Switch System with Nonlinear Actuator Faults, *International Journal of Fuzzy* , vol. 23, no. 7, pp: 2297-2308, 2021.

[38] P. Baranyi, T–P model transformation as a way to LMI–based controller design, *IEEE Transactions on Industrial Electronics*, vol. 51, no. 2, pp: 387–400, 2004.

[39] M. E. *Basoğlu*, B. Cakir. Comparisons of MPPT performances of isolated and nonisolated DC–DC converters by using a new approach, *Renewable and Sustainable Energy Reviews*, vol. 60, pp: 1100–1113, 2016.

[40] R. W. Erickson, D. Maksimovic. Fundamentals of Power Electronics, *Springer, New York, USA*, 2001.

[41] K. Tanaka, H. Wang, Fuzzy Control Systems Design and Analysis: A Linear Matrix Inequality Approach, *John Wiley & Sons, New York*, 2002.

[42] C. Peng and T. C. Yang, Event-triggered communication and H_∞ control co-design for networked control systems, *Automatica*, vol. 49, no. 5, pp. 1326–1332, 2013.

[43] E. G. Tian and D. Yue, Reliable H_∞ filter design for T–S fuzzy modelbased networked control systems with random sensor failure, *International Journal Robust Nonlinear Control*, vol. 23, no. 1, pp. 15-32, 2013.

[44] J.W. Wang, H.N. Wu, L. Guo, Y.S. Luo. Robust H_∞ fuzzy control for uncertain nonlinear Markovian jump systems with time–varying delay, *Fuzzy Sets and Systems*, vol. 212, pp: 41–61, 2013.